Coastal Engineering 180 (2023) 104271

Contents lists available at ScienceDirect

Coastal Engineering

journal homepage: www.elsevier.com/locate/coastaleng

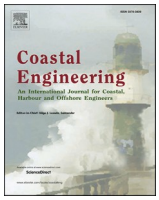

Multimodal harbor wave climate characterization based on wave agitation spectral types

Eva Romano-Moreno *, Gabriel Diaz-Hernandez, Antonio Tomás, Javier L. Lara

IHCantabria - Instituto de Hidráulica Ambiental de la Universidad de Cantabria, Santander, Spain

ARTICLE INFO

Keywords:
Harbor wave climate
Harbor wave agitation
Multimodal waves
Directional wave spectra
Wave spectral types

ABSTRACT

A new numerical methodology reaching an improved characterization of the historical harbor wave agitation climate is presented in this work. A detailed frequency-direction wave spectrum definition of wave agitation patterns within harbor basins is achieved, providing an in-depth description of the whole multidirectional and multireflective wave patterns occurring as a natural harbor response. This constitutes an advance from the monoparametric/aggregated wave height parameter-based approaches, traditionally used for wave agitation characterization, to a multivariate and disaggregated representation of in-port waves and the multiple wave transformation processes within harbor basins. In addition, the wave agitation spectral type concept is proposed, whereby the wave agitation spectral shapes are classified into representative clusters of the historical wave agitation response in a harbor. A detailed multiannual analysis of the wave agitation response, based on the different in-port spectral wave components, their relation with the outer-harbor forcing waves, and their interactions with the harbor structures, can be achieved with the proposed methodology. This improved harbor wave climate characterization can be especially relevant for port operability and downtime analyses. The methodology is applied and validated in Africa basin (Las Palmas Port, Spain).

1. Introduction

A suitable characterization of harbor wave climate is the basis for many engineering applications, especially for practical harbor operability/downtime analysis. As a common practice, harbor wave climate characterization is usually based on aggregated parameters (mainly, zero-order moment spectral wave height, Hm_0; peak period, Tp; and harbor resonance frequencies). Different criteria defining recommended operational/downtime limits are based on the exceedance of wave height thresholds for different types of ships (ROM3.1-99, Puertos del Estado, 1999; Thoresen, 2003; PIANC, working group PTC II-24, 1995).

In harbor areas, highly multidirectional wave patterns result from a complex interaction of outer waves penetrating and interacting with the harbor structures, mainly by a combination of wave diffraction processes with successive (re-)reflected wave trains at the inner port contours. In addition, an important spatial variability of the in-port wave climate arises due to complex harbor configurations (mainly geometry, perimeter dissipation capacity and bathymetry characteristics). Remarkable energy, spectral wave frequency and/or directional variations can occur at different in-port locations. These complex effects are translated into an equally complex definition of the wave energy distribution within the harbor basin. Because of this spatial, multicomponent and multiparameter variability of waves inside a harbor, a monoparametric-based approach is insufficient; a frequency-direction spectral definition of wave agitation is required for an adequate description of the multimodal harbor climate. In this way, the wave agitation patterns, usually defined by the aggregated value of total wave height, can be disaggregated into its multiple frequency and directional wave components.

This improved characterization of harbor climate can be particularly relevant for port operability/downtime studies in terms of both wave height and moored ship motions (Cornett et al., 2012; Demenet et al., 2018; Pinheiro et al., 2013; Sakakibara and Kubo, 2008; Van der Ven, 2012), where beyond the scalar magnitude, the influence of the wave energy is determined by the spectral frequency-direction wave energy distribution. It can also be of particular importance for detailed assessment of wave energy potential (Iglesias et al., 2009; Mørk et al., 2010; Vicinanza et al., 2013) in areas affected by wave reflection from natural

* Corresponding author.
E-mail addresses: eva.romano@unican.es (E. Romano-Moreno), gabriel.diaz@unican.es (G. Diaz-Hernandez), antonio.tomas@unican.es (A. Tomás), jav.lopez@unican.es (J.L. Lara).

https://doi.org/10.1016/j.coastaleng.2022.104271
Received 14 June 2022; Received in revised form 17 November 2022; Accepted 15 December 2022
Available online 17 December 2022

or artificial structures, as well as for future infrastructure designs.

Nevertheless, at present, the complete wave spectral definition within harbor areas is not commonly carried out for both numerical models and on-site measurements. Different methods exist for estimating the directional wave spectrum from measured data, either in physical models in the laboratory or on-site locations (Benoit et al., 1997). However, on-site measurements are not commonly available due to the high cost entailed and the complexity in deploying the instrumental equipment, which can also interfere with ship navigation and harbor activities. Similarly, laboratory setups for harbor agitation studies are not commonly carried out in practice, either, mainly due to the high cost, scale limits and assembly complexity for different geometries and modifications. Available laboratory experiences can be found in van der Ven et al. (2018), where integrated variables of irregular wave trains are measured, but not the full spectrum. Additionally, the lack of interest in measuring the directional spectrum within harbor areas, either in the laboratory or real situations, may lie in the lack of a real need for this additional information, since the traditional analysis and validation methodologies have always been based on single-parametric approaches, as explained above. However, this approach is expected to change due to the current ability to numerically model the complete wave spectrum characteristics from deep waters to coastal zones and outer harbor areas. In recent years, advanced third-generation spectral wave models, such as SWAN (Booij et al., 1999) and WAVEWATCH-III (Tolman, 1991), have been used to solve the full wave spectrum, yielding real-shaped multimodal (multipeaked) spectral shapes and thus better wave climate characterization. Indeed, one of the latest advances in numerical wave agitation modeling lies in more accurate outer-harbor spectral wave climate definitions achieved by using these spectral wave models (Diaz-Hernandez et al., 2021). An important uncertainty reduction in wave agitation prediction can be achieved by using an accurate spectral wave climate characterization in the vicinity of the harbor (Romano-Moreno et al., 2022). However, the capability of these types of numerical models decreases due to the physical processes involved in wave propagation and penetration in harbor areas (Dusseljee et al., 2014; Eikema et al., 2018; Enet et al., 2006; Holthuijsen, 2007; Holthuijsen et al., 2003; Ilic et al., 2007; Rusu and Soares, 2013; Violante-Carvalho et al., 2009). The so-called phase-resolving numerical models, either based on the elliptic mild-slope (e.g. CGWAVE, Panchang and Xu, 1995; HARBD, Chen and Houston, 1987; Chen and Mei, 1974; HARES, Svašek Hydraulics, n.d.; MIKE21 EMS, DHI, 2017; MSP, Diaz-Hernandez et al., 2021; GIOC, 2007; and PHAROS, Deltares, n.d.; Hurdle et al., 1989; Kostense et al., 1986) or Boussinesq equations (Brocchini, 2013) (e.g. BOUSS-2D, Nwogu and Demirbilek, 2001; FUNWAVE, Kirby et al., 1998; Shi et al., 2016; MIKE21 BW, DHI, 2022; and TRITON, Borsboom et al., 2000), are the most appropriate and commonly used models for wave agitation assessment (Eikema et al., 2018; Gruwez et al., 2012; Liu and Losada, 2002; Rusu and Soares, 2013; Violante-Carvalho et al., 2009).

Originally, the directionality of waves is not directly solved with these classes of wave models. Indeed, different works can be found in the literature addressing the computation of this required wave characteristic to fulfill the boundary (partial) reflection condition for elliptic mild-slope-based prediction of wave propagation (Beltrami et al., 2001; Isaacson et al., 1993; Isaacson and Qu, 1990; Steward and Panchang, 2001). These methods mainly consist of estimating the approaching (bulk) direction of waves in monochromatic wave fields based on the gradient of phase or free surface elevation function (Beltrami et al., 2001; Isaacson and Qu, 1990; Steward and Panchang, 2001) or the tangential component (Isaacson et al., 1993). Following the same phase gradient-based approach, a progress towards spectral waves is presented in De Girolamo (1995). In that work, an expression is proposed, under the assumption of linear theory, to evaluate the representative mean wave direction of a spectral wave field solved through a mild-slope-based model, related to the overall energy flux direction. In this way, an aggregated parameter representative of the mean direction of wave propagation is estimated throughout the entire numerical domain. Theoretically, the phase gradient-based approach used in this method is only applicable to progressive waves, and not to surface elevations composed of multiple wave components (Beltrami et al., 2001). Nevertheless, adequate estimations are obtained in weak reflection scenarios (Beltrami et al., 2001) and defining random directionally spread waves (De Girolamo, 1995).

As stated above, aggregated parameters are insufficient and the directional wave spectrum definition is an indispensable requirement for a disaggregated characterization of the wave agitation climate in a harbor. As previously mentioned, different methods exist for estimating the directional wave spectrum from measured wave field data, either in laboratory physical models or at on-site ocean locations, mainly based on linear analysis for open water conditions (Barstow et al., 2005; Benoit et al., 1997). These methods usually rely on the simultaneous measurements of wave field characteristics (related to or the surface elevation itself) at one (e.g. single-point devices) or several (e.g. gauge arrays) positions. Many of them are based on the classical Directional Spreading Function (DSF) approach, which consist of representing the complete directional wave spectrum (E(f, θ)) as the product of the scalar frequency spectrum (S(f)) by a DSF describing the directional distribution (D(f, θ)) of the spectral wave energy, as follows: $E(f,\theta) = S(f)\cdot D(f,\theta)$. Different analysis methods exist to estimate the DSF (e.g. Fourier series decomposition methods, parametrical models, Maximum Likelihood Methods, Maximum Entropy Methods, or Bayesian Directional Method; Benoit et al., 1997). A comprehensive review of such commonly used methods is presented in Benoit et al. (1997). However, these methods are commonly based on parametrized or theoretical definitions of the DSF, which are insufficient or limitedly capable for representing the shape of the wave energy distribution/peaks in some real situations, mainly when dealing with multimodal waves. Furthermore, the standard methods mentioned so far are stochastic methods (i.e., the wave phase parameter is assumed as randomly distributed), which makes these methods unsuitable for use in scenarios with wave reflection (because of the phase-locking between wave components; Benoit et al., 1997), such as harbor basins. Modifications or extensions of those standard methods aimed at estimating the directional wave spectrum in reflective scenarios can be found in the literature (e.g. Davidson et al., 1998; Hashimoto and Kobune, 1987; Isobe and Kondo, 1985; Yokoki et al., 1995). They are presented applied to laboratory and on-site measured data, mainly based on analyses of typical reflection patterns such as in front of a structure (rubble mound or vertical breakwater). Some limitations and required advances/optimizations for some of these modified methods are mentioned in Teisson and Benoit (1995) and Huntley and Davidson (1998). A variation of an standard method including wave diffraction is presented in Song et al. (2022). Another class of directional analysis approaches, keeping the wave phase information, are deterministic analysis methods (Benoit et al., 1997; Panicker and Borgman, 1970; Sand, 1979, 1984; Schäffer and Hyllested, 1994). These are based on the representation of the surface elevation as a superposition of regular wave components with different amplitude, frequency, direction and phase parameters. Through these methods, the direction and complex amplitude (wave amplitude and phase) of each considered wave component in the wave field are estimated in such a way their total superposition coincides with the measured surface elevations in terms of the complex Fourier coefficients (Benoit et al., 1997; Janssen et al., 2001). Finally, hybrid approaches combining the application of first stochastic and then deterministic methods are presented in Janssen et al. (2001), Prislin et al. (1997), and Prislin and Zhang (1996). They are intended for complete characterization (including wave phase) of multiple predefined wave components identified from an initially estimated stochastic-based DSF. In principle, an unlimited number (although depending on the number of gauges) of directional wave components per frequency can be addressed with these methods. However, fewer and more spread wave components may be expected to be identified from the smoothed shapes of DSF-based directional wave spectra than one

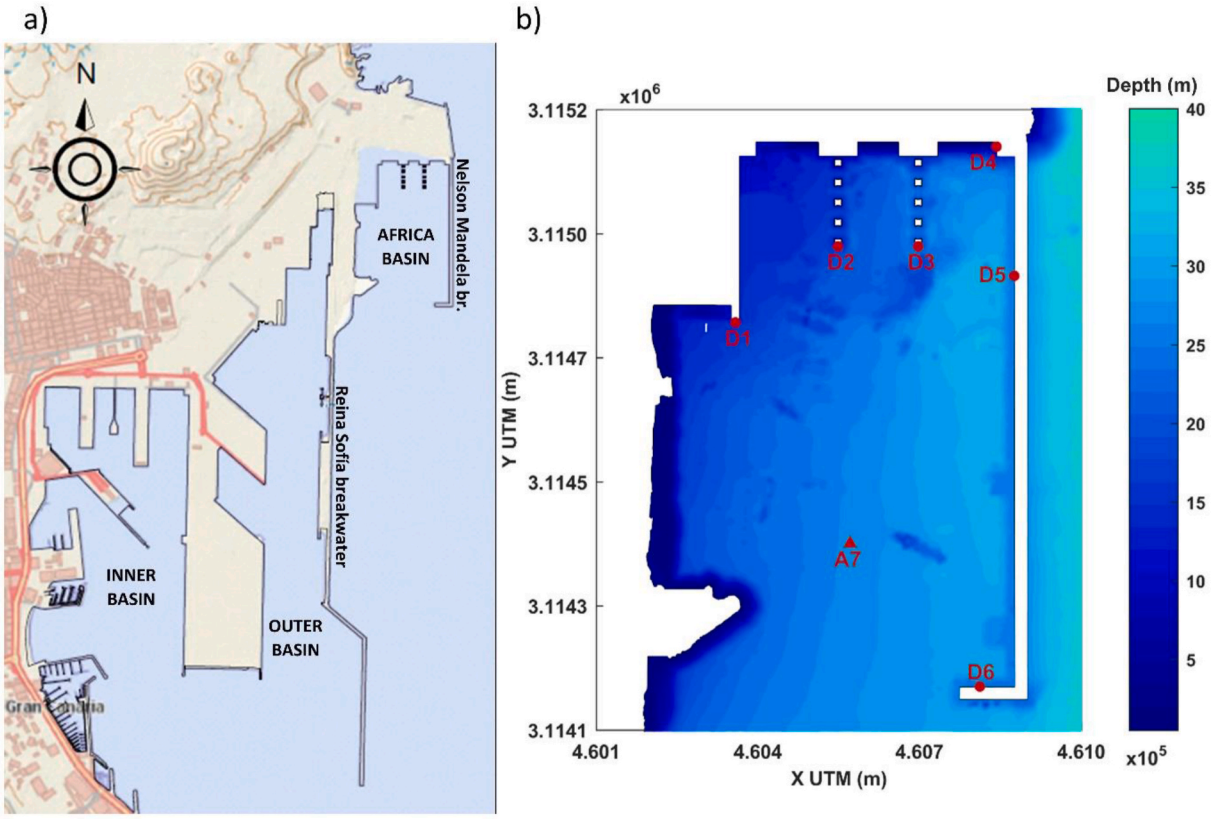

Fig. 1. a) Location of Africa basin in Las Palmas Port. Actual port geometry. Source of base map: viewfinder Grafcan (IDE Canarias, Government of the Canary Islands). b) Location of measuring systems in Africa basin (DeepWAVES: D1 to D6, AWAC: A7). UTM coordinates (m). Actual bathymetry (m). Source: Romano--Moreno et al. (2022).

component per frequency-based deterministic approaches (Benoit et al., 1997). Another such considered approach applied in multidirectional experimental waves is presented in Draycott et al. (2016). Based on a single-summation method, incident wave direction per frequency is calculated in a first step avoiding phase-locking. An in-line incident/reflected wave separation analysis is performed in a second step, focused on the subsequent calculation of the incident and reflected wave directional spectra. This method is limited to the assumption of wave reflection mirroring the incident waves and oblique wave reflection processes are not solved (Draycott et al., 2016).

In summary, a wide variety of methods for directional wave spectrum estimation can be found in the literature, but none of the methods described so far have been specifically developed to be used in multi-reflective (highly multimodal) patterns such as those occurring in ports. In addition, as mentioned above, most of the methods are based on measured information either in physical models or at on-site locations. This conflicts to some extent with the priority of relying on numerical modeling for wave agitation assessment. Therefore, new methods or extensions of those mentioned above are required enabling the calculation of directional wave agitation spectra in harbors from numerical modeling-based approaches and more specifically through phase-resolving wave models. A small number of works focused on this purpose can be found in the scientific and technical literature. Indeed, to the knowledge of the authors of the present paper, the specific purpose of reconstructing the directional wave spectrum within harbor areas is uniquely fulfilled by the WAVEDIRECT (Svašek Hydraulics, 2019) postprocessing tool. It was recently implemented in the elliptic mild-slope numerical model HARES (Svašek Hydraulics, n.d.), which is able to detect wave directions within the model results and build the directional spectra. An application case of this tool in a real harbor is shown in Svašek Hydraulics (2019). However, no further references of this postprocessing technique applied to real harbor analysis and climate assessment have been found in the literature. The postprocessing method (rotating Directional Phase Resolving Analysis, r-DPRA) proposed by de Jong and Borsboom (2012) addresses the problem by estimating directional wave components derived from monochromatic wave fields resulting from phase-resolving models. This is not a method to directly reconstruct the directional wave spectra, but rather to identify the arbitrary multidirectional wave components in a single-frequency wave field. In contrast to phase gradient-based methods, a comprehensive wave description (separate wave heights, directions and phases) per frequency is provided by r-DPRA, instead of a bulk mean direction. The postprocessing r-DPRA method applied for regular wave propagation within simplified harbor configurations or theoretical/academic scenarios is presented in de Jong and Borsboom (2012) and Oude Vrielink (2016). The r-DPRA applied in spectral wave propagations can be found in de Jong et al. (2016) for unidirectional estimations of the main/incoming wave direction in a port entrance channel, or considering a single spectral component for directional analysis in an array configuration of wave energy converters in van der Wiel et al. (2016). In Van Essen et al. (2013), the r-DPRA method is used with the aim of reconstructing the long wave directional spectrum in an open LNG terminal from synthetic series of free surface. Overestimation of directional spreading, which is estimated based on the total energy per frequency and the analysis resolution, is reported. For the present research, the r-DPRA method is applied, within a monochromatic propagation framework, with the further objective of reconstructing historical series of frequency-direction wave agitation spectra within harbors by means of spectral reconstruction techniques subsequently applied in an hourly and dynamic approach. As explained in the methodology section, in this work, the spectral wave energy distribution arises from the contribution of each energy sub-component to each

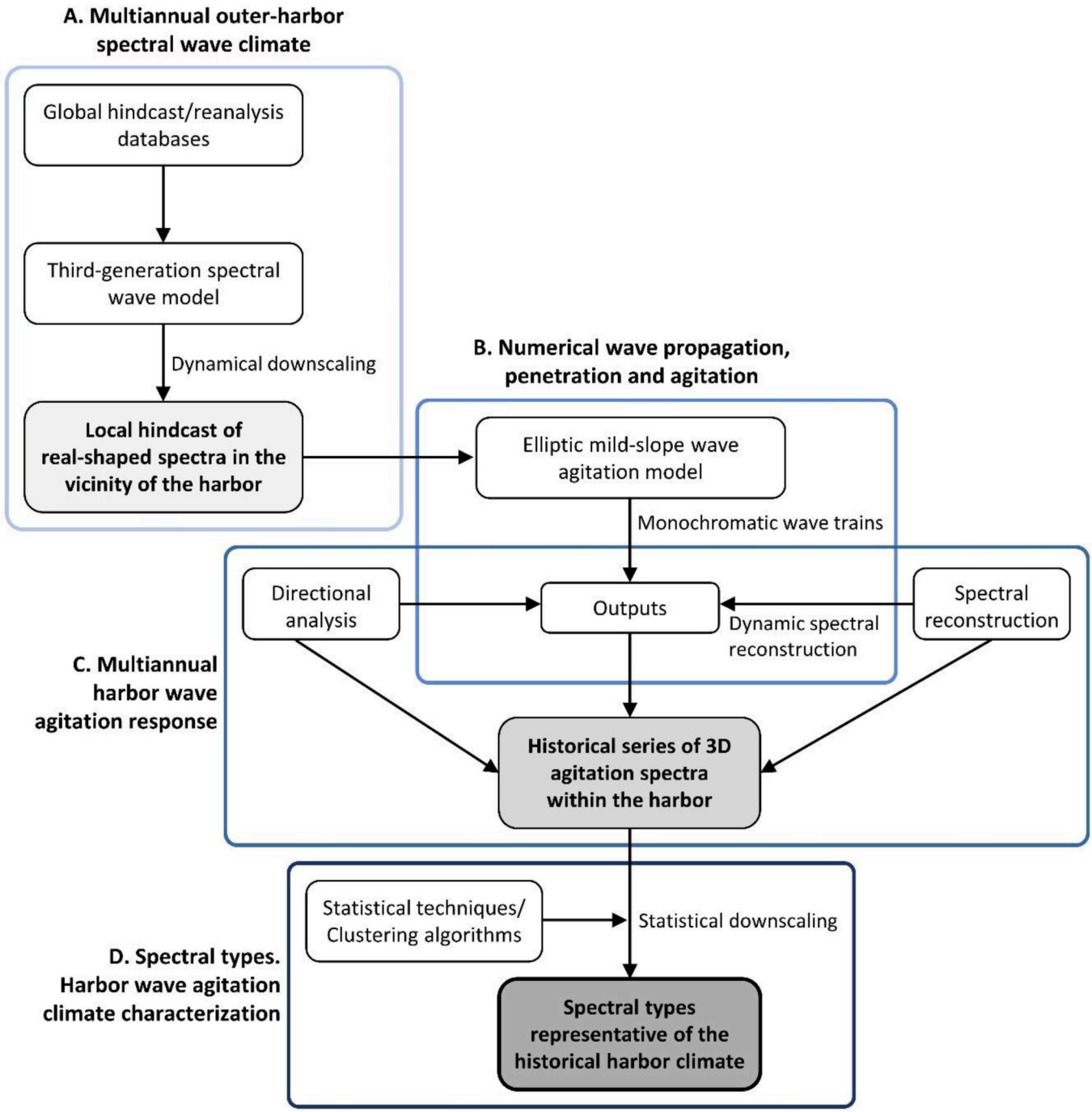

Fig. 2. General scheme of the methodology.

frequency-direction pair in the initial discretized spectrum.

This proposed progress in wave characterization, allowing the complete wave agitation spectrum definition, could become inconvenient due to the increased complexity for statistical postprocessing and assimilation of multiyear time series of disaggregated variables. This problem is addressed in the present paper through an effective characterization of the historical spectral wave agitation response based on representative spectral types (hereafter ST), which is the final objective of this paper.

The concept of pattern-type definition consists of a clustering into a reduced number of representative cases for large datasets of historical data. Clustering algorithms applied to long time series of waves defined by sets of aggregated parameters are presented in Camus et al. (2011). A parameter-based procedure for spectral classification according to the number of peaks and the distance between them in directional spectra is proposed in Boukhanovsky et al. (2007). From an initial partitioning of directional spectra, a methodology to cluster the historical partitioned wave systems, based on their probability of occurrence, by grouping the frequency-direction peaks and assimilated to a kind of spectrum was proposed in Portilla-Yandún et al. (2015). More recently, a classification of wave spectra based on clustering algorithms was performed in Espejo et al. (2014), applied to daily deep-water buoy data to statistically relate atmospheric/weather and spectral types. To our knowledge, no references have been found focused on obtaining a climate analysis based on a detailed characterization of multimodal spectra within harbors, nor have studies using classification and/or clustering techniques for harbor

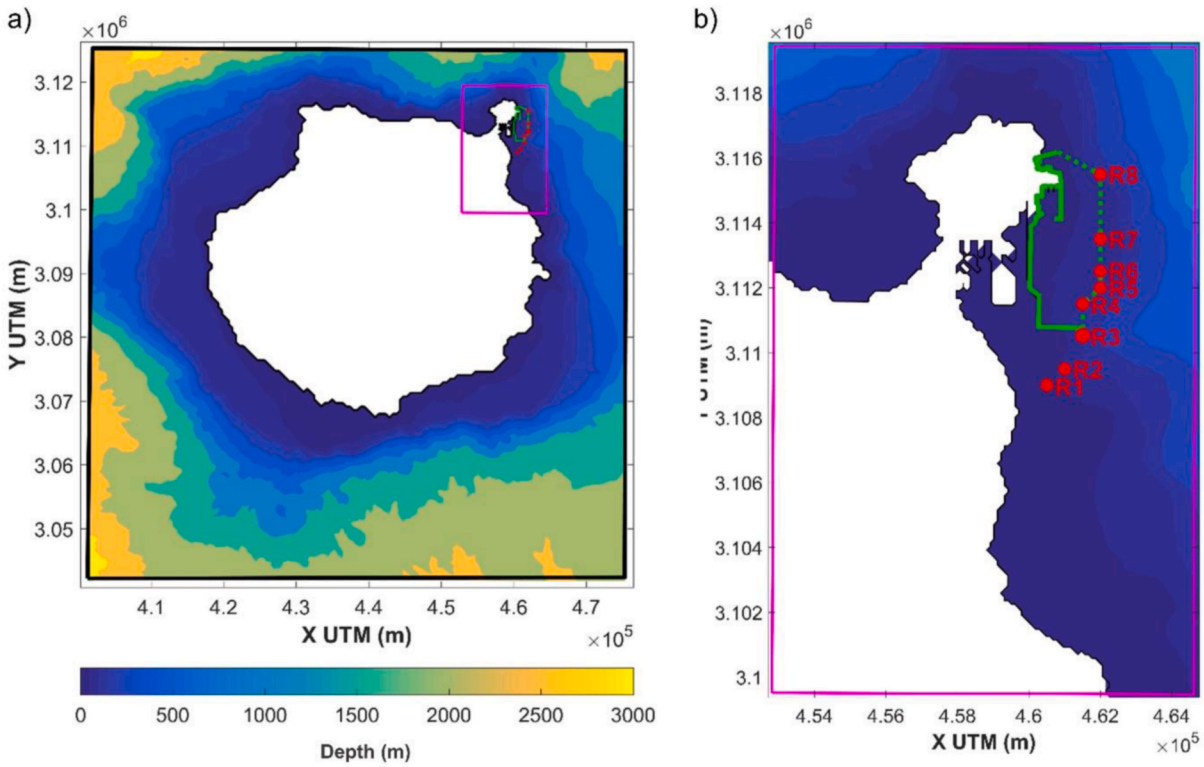

Fig. 3. a) Numerical grids defined in SWAN. Low resolution (black): dx = dy = 0.005°; Fine resolution (magenta): dx = dy = 0.001°. Numerical domain in MSP (green). b) Numerical domain in MSP within the fine grid in SWAN. Position of forcing points in MSP (R1–R8). UTM coordinates. Actual bathymetry (m). Source: Romano-Moreno et al. (2022).

wave agitation databases been found.

In this research, the wave agitation processes influencing the in-port wave climate are assessed through comprehensive numerical and statistical analyses. Accordingly, the long-term spectral wave agitation climate is effectively described by a reduced number of representative frequency-direction spectral patterns, allowing a simpler interpretation of the spatially variable wave agitation response in a harbor.

The disaggregation of the hourly historical wave agitation patterns, at any position inside the harbor, into the n-modal directional wave agitation spectra is the first objective of the methodology. The statistical assimilation of the hourly and multiyear wave agitation spectra at each in-port target position for the subsequent ST clustering is the second objective of the methodology. After ST clustering and representation, the in-port spectral wave climate is efficiently described and related to the outer-harbor spectral wave climate.

In summary, a multidimensional analysis based on a spectral wave agitation description is proposed, in contrast to single-parameter-based approaches. An important advance for future harbor downtime analyses can result from this new approach, extending the classical monoparametric/scalar approaches to a multiparametric/directional one.

This paper is organized as follows: A brief description of the study port area (Africa basin, located in Las Palmas Port, Canary Island, Spain) and the field measurements used for the validation procedure is presented in Section 2. In Section 3, the methodology, divided into separate steps, is described and validated, including a brief description of the historical multimodal wave climate in the vicinity of the study site. In Section 4, the methodology is applied and validated with on-site measured data in the study port area, where some interesting multimodal in-port wave agitation patterns are induced due to the highly multimodal outer-harbor wave climate, influenced by the geometry of the harbor. Finally, the main conclusions are summarized in Section 5.

2. Study port area and field data used for validation

The methodology proposed in this work has been applied in a real port area, Africa basin (Fig. 1a), located in Las Palmas Port (Canary Islands, Spain). This infrastructure is facing the Atlantic Ocean with a south-oriented harbor entrance. Two main boundary structures shelter the harbor: the Nelson Mandela breakwater on the eastern side and the Reina Sofia breakwater on the western side. The former is mainly a vertical structure, approximately 1000 m long, made of concrete caissons. Two different breakwater cross-sections of approximately 1600 m and 1400 m long can be identified in the latter. A rubble mound breakwater is formed on the first north-south oriented section, and a concrete vertical structure is formed on the final section. Caisson-made vertical quay walls predominate as inner contours in the basin, with sloped rubble mound cross-sections between concrete berthing ramps on the north side. A natural slope and fills conform to the unbuilt inner-western contour of the basin. A maximum water depth of 35 m, at high water level (tidal range of 3 m), is registered in the basin (Fig. 1b).

The numerical results obtained in this study have been validated with 8-month instrumental data acquired from a field campaign undertaken in this basin from July 2019 to February 2020. A spectral wave single-parameter validation has been performed with data from 6 wave agitation gauges located at different positions within the basin (points D1 to D6 in Fig. 1b). The free surface was measured for 20-min periods every hour by DeepWAVES devices (ultrasonic range finders) with a sampling rate of 5 Hz. Postprocessed hourly scalar spectral variables have been used for this validation. Additionally, postprocessed scalar and multidirectional information from 1-month instrumental data from an Acoustic Wave and Current Profiler with Acoustic Surface Tracking (AWAC-AST, Nortek AS; point A7 in Fig. 1b) have been used for directional validation. A pressure and velocity sampling rate of 2 Hz, and 4 Hz for surface tracking (Nortek, 2017) were used by the AWAC system.

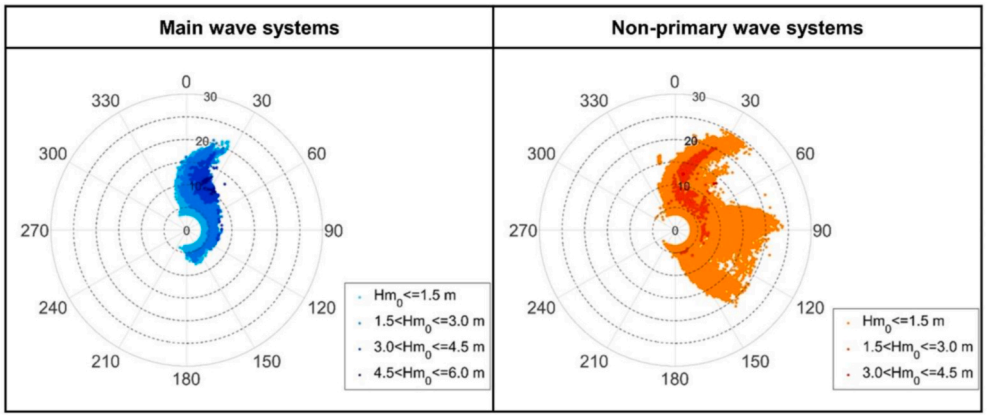

Fig. 4. Hm_0 of the main and secondary wave systems from partitioned historical spectra at point R6 represented in a Tp period-Dm direction space in polar plots. Different wave height values are represented by color scales.

3. Methodology

The overall methodology proposed to generate the new ST-based climatic analysis for an improved definition of the harbor agitation climate is presented in this section.

The complete methodology (Fig. 2) is composed of the following steps:

A. Multiannual outer-harbor spectral wave climate characterization based on historical hourly wave datasets of local real-shaped wave spectra.
B. High-resolution numerical wave propagation, penetration and wave agitation inside the harbor.
C. Multiannual harbor wave agitation response characterization based on historical series of directional wave agitation spectra.
D. Spectral types (ST) definition of harbor wave agitation climate at any point inside the basin.

The proposed methodology begins with the dynamic wave downscaling strategy for harbor agitation assessment described in Romano-Moreno et al. (2022), where steps A and B were already developed and validated with on-site measured data in Africa basin. Steps C and D are described in Sections 3.3 and 3.4, respectively, yielding a comprehensive characterization of the historical spectral wave agitation response.

The historical and full spectral approaches taken throughout the entire methodology should be pointed out. A complete dynamic downscaling is conducted, i.e., from the generation of hourly multiannual (hindcast) series of the real-shaped spectra in the vicinity of the harbor to the mathematical reconstruction of the historical series of hourly directional wave agitation spectra at different in-port target points. This means that a consistent representation of all the relevant physical processes involved in wave propagation and penetration into a harbor is achieved.

The different steps are described in the following subsections as they are applied in the study port area (Africa basin).

3.1. Multiannual outer-harbor spectral wave climate characterization based on historical series of local real-shaped wave spectra (A)

An accurate characterization of the multimodal spectral wave climate outside the port is already achieved in Romano-Moreno et al. (2022) based on a real-shaped wave spectra definition approach. By means of dynamic wave downscaling from offshore to near-port, the 40-year historical time series of hourly real-shaped directional spectra (with a 41 × 48 frequency-direction discretization) are generated at 8 different positions (points R1-R8 in Fig. 3b) in the vicinity of the port. Points R1-R8 are defined to characterize the spatial variability of outer-port wave climate since this historical information is used as forcing for the subsequent wave agitation modeling.

Numerical wave propagation from offshore deep waters to the vicinity of the port is accomplished by using the third-generation spectral wave model SWAN (Booij et al., 1999). Hourly and non-stationary wave simulations are performed following a dynamic wave downscaling approach. Hindcast/reanalysis data of spectral waves (Global Ocean Waves (GOW2) (Perez et al., 2017)), wind (Climate Forecast System (CFSR) (Saha et al., 2010), (CFSv2) (Saha et al., 2014)) and sea level (Global Ocean Tide (GOT) (IHCantabria, based on the TPXO global tides model (Egbert et al., 1994; Egbert and Erofeeva, 2002); and Global Ocean Surges (GOS) (Cid et al., 2014)) are used to force the SWAN model. A spatial resolution of 0.001° is reached in the study port area for the fine resolution mesh defined in the numerical model (Fig. 3). A robust wave validation of this first step of the methodology is presented in Romano-Moreno et al. (2022), based on instrumental data from offshore and coastal buoys located at different positions throughout the numerical domain. Further details about the wave downscaling strategy and validation process are described in Romano-Moreno et al. (2022).

A strongly multimodal wave climate prevails in the near-port area of Africa basin. From a statistical analysis of the historical wave climate at point R6, presented in Romano-Moreno et al. (2022), 18.4% of the hourly historical sea states correspond to unimodal wave spectra, while the remaining 81.6% present multimodal spectral shapes comprised by two or more wave components or modes. In a ranking, 27.4%, 26.7%, 19.3% and 8.2% of historical sea states correspond, respectively, to bimodal, trimodal, 4-peaked and 5-peaked spectral shapes.

Parameterized main and non-primary partitioned wave systems from historical real-shaped spectra at point R6 are presented in Fig. 4. As a brief characterization of the historical wave climate outside the port, mean wave directions (Dm) coming from the NNE, Tp between 5 and 10 s and Hm_0 up to 3 m are the predominant main wave system conditions to which Africa basin is exposed. As the multimodality of waves increases, Hm_0 decreases to below 1.5 m for practically all non-primary wave systems; predominant Tp is between 10 and 15 s for northeastern wave directions, while 5–7.5 s is the most likely Tp range for southeastern wave directions. A more detailed characterization of the multimodal wave climate in the vicinity of Africa basin is presented in Romano-Moreno et al. (2022).

3.2. High-resolution numerical wave propagation, penetration and wave agitation inside the harbor (B)

This second step of the methodology addresses the spectral wave climate propagation from outer-harbor locations to inside the basin. The approach adopted to this end is based on the accurate dynamic wave downscaling strategy for wave agitation assessment described in

Romano-Moreno et al. (2022). The improved model MSPv2.0 (Diaz-Hernandez et al., 2021) is used for numerical wave propagation and wave agitation modeling. This modified elliptic mild-slope-based model provides an efficient numerical model for high-resolution wave propagation in large harbor areas. Additionally, dynamic reflection coefficients (Kr) varying as functions of incident wave periods (T) can be defined for each harbor contour. The actual port configuration perimeter and the detailed bathymetry in the study area are defined in a numerical domain of 2.0 km width × 5.4 km length (Fig. 3). Dynamic Kr(T) curves are defined for 20 different port contours/structure typologies, based on the treatment proposed by Vílchez et al. (2016), according to the real cross-section characteristics. Historical series of real-shaped outer spectra previously generated at points R1-R8 are used as forcing spectral wave climate for wave agitation modeling. Historical hourly spectral wave agitation predictions are dynamically obtained by following the monochromatic-based approach described in Diaz-Hernandez et al. (2015) and Diaz-Hernandez et al. (2021). This is an efficient numerical approach to be adopted in a dynamic wave agitation downscaling strategy, such as the current one, for long-term wave agitation assessment. From a defined catalog of monochromatic wave propagations with MSPv2.0, the spectral wave agitation, in terms of wave height, is reconstructed as a superposition of energy-transformed agitation maps of monochromatic waves comprising each discretized real-shaped forcing spectrum. A 36 × 72 frequency-direction monochromatic catalog is used in this work. The good predictive behavior of this numerical approach, applied in the study Africa basin, is presented in Romano-Moreno et al. (2022) with high correlation coefficients obtained from a comparison of numerical wave agitation results with on-site measured data during the field campaign at 7 control points (D1-D6, A7 in Fig. 1b). From this accurate dynamic wave agitation downscaling procedure, the 40-year historical series of hourly spectral agitation maps are obtained, allowing an improved characterization of the historical wave agitation response of the study port basin in terms of in-port Hm_0.

3.3. Multiannual harbor wave agitation response characterization based on historical series of directional wave agitation spectra (C)

From validated wave agitation modeling, this step of the methodology is aimed at achieving a frequency-direction spectral-based definition of harbor wave agitation, allowing to advance from an aggregated/monoparametric to a disaggregated/multidimensional characterization of long-term wave agitation response in a harbor area.

The total wave agitation throughout the entire numerical domain, in terms of aggregated Hm_0, is provided by the spectral agitation maps previously reconstructed as explained in Diaz-Hernandez et al. (2021). In turn, the inner-harbor numerical results from propagations of monochromatic waves provide aggregated representations of different incoming, diffracted and reflected wave subcomponents coexisting inside the harbor basin without a clear definition of wave directions and wave agitation patterns. Such monochromatic directional wave subcomponents comprising the wave agitation maps provided by the numerical MSPv2.0 model can be identified by using the r-DPRA method. This method allows to determine the individual directional wave patterns within the multidirectional single-frequency wave fields resulting from a phase-resolving wave model.

The r-DPRA is an extension of the original Directional Phase Resolving Analysis (DPRA) method previously developed in Janssen et al. (2001). Based on linear theory, the method assumes that the free surface elevation in a short-crested wave field is represented as a superposition of a finite number of multidirectional long-crested regular waves with different amplitudes and phases. By using a classical Fourier analysis (Eq. (1)), for a specific frequency (n) and from free surface elevation values at several positions (p) around a target point (r), each directional wave system (v = 1 to L) can be estimated in such a way that the superposition of all of them results in the known free surface.

$$b_{n,p} = \sum_{v=1}^{L} exp\left(ik_{n,v} \cdot \left(x_p - x_r\right)\right) z_{n,v} + \varepsilon_{n,p} \quad (1)$$

where $k_{n,v}$ denotes the wavenumber vector in each direction v; x_p and x_r refer to gauge and reference points, respectively; $z_{n,v}$ is the Fourier coefficient for each individual frequency-direction component; and $\varepsilon_{n,p}$ represents the inaccuracies/deviations introduced due to the assumed simplifications (Janssen et al., 2001).

A set of directions for analysis is defined, assuming that waves are propagating in such directions. By means of the least-squares method, the Fourier coefficients (amplitude and phase) of the individual wave system for each direction are calculated with the minimum deviation ($\varepsilon_{n,p}$) between the estimated and known free surface elevation initial values. The original DPRA method is applied after a phase-averaged method for a previous estimation of directional distribution (Janssen et al., 2001). The improved r-DPRA extends the method without taking into account the predefinition of the directional distribution of waves. For this purpose, the monochromatic wave phase must be solved by the numerical wave agitation model as the complex free surface elevation equation. In this case, the set of analysis directions is rotated in angular increments, and the directional analysis is solved at every rotation step. The resolution of the method increases with the number of analyzed directions, up to a certain extent for which too many fictitious components result. The final directional solution is chosen for the optimum energy configuration integrated over the entire circumference (de Jong and Borsboom, 2012).

For this research, an in-house postprocessing tool based on the r-DPRA method has been developed to obtain the different directional wave subcomponents comprising the monochromatic wave fields obtained using the MSPv2.0 model. For each monochromatic wave in the predefined catalog, the directional analysis is solved from the complex amplitude values of free surface in a number of numerical nodes around the target locations within the basin. A homogeneous wave field and constant water depth are assumed in each analysis area. The directional wave subcomponents at different basin locations for each monochromatic case are subsequently used for the dynamic historical reconstruction of hourly directional agitation spectra within the harbor. In this way, spectral reconstruction techniques are applied to the monochromatic directional wave subcomponents to estimate the multimodal wave agitation spectra in real harbor configurations. In this approach, wave energy spreading within each spectral subcomponent is not solved, but the energy distribution/spreading of a reconstructed spectrum arises from the contribution of each energy subpackage to each frequency-direction pair in the initial discretized spectrum. By using spectral reconstruction techniques, every energy component of an irregular sea state outside the harbor is transformed and disaggregated in its multiple contributions to the corresponding energy packages comprising the in-port agitation spectrum. The real-shaped wave spectra, previously generated in the vicinity of the port (Section 3.1), are used as forcing for the wave agitation spectra reconstruction. By using a dynamic approach, the historical series of hourly directional agitation spectra are generated at different locations within the basin.

As a first validation of the method for directional spectra reconstruction, the hourly real-shaped wave spectra near the wave generation contour of the numerical domain defined in MSPv2.0 have been reconstructed for the 8-month period of the field campaign in Africa basin. This reconstruction procedure has been performed from monochromatic wave propagations considering the entire harbor geometry defined as absorbing contours and constant maximum water depth. Thus, only incident waves exist within the numerical domain, and any wave reflection or interference is avoided. The numerically reconstructed spectra have been compared to the initial forcing spectra. Since the MSPv2.0 model is an extensively validated model for wave agitation assessment (Diaz-Hernandez et al., 2021), and assuming the deviations introduced by the MSPv2.0 model are negligible, this first comparative

Table 1
Main statistical and correlation coefficients from comparison between initial and reconstructed directional spectra near the wave generation contour in the numerical domain defined in MSPv2.0. Visualization of the accuracy of the method for directional spectra reconstruction. Aggregated spectral wave parameters; separate spectral parameters for the three main wave systems from spectral partitioning. Wave parameters: Hm_0; spectral mean wave period (s), defined from zero- and second-order spectral moments (Tm_{02}); Tp; Dm; Dp: peak direction (°).

Parameterization approach	Parameter	BIAS	RMSE	SI	CORR	R^2	Rc
Aggregated	Hm_{0_ag}	−0.005 m	0.006 m	0.005	1.00	1.000	–
	Tm_{02_ag}	0.020 s	0.041 s	0.007	1.00	0.999	–
	$Tp_{\_ag}$	0.019 s	0.103 s	0.011	1.00	0.999	–
	$Dm_{\_ag}$	–	–	–	–	–	0.999
	$Dp_{\_ag}$	–	–	–	–	–	0.995
Main partitioned wave system	Hm_{0_1}	−0.021 m	0.038 m	0.032	1.00	0.994	–
	$Tp_{\_1}$	0.015 s	0.062 s	0.008	1.00	0.999	–
	$Dm_{\_1}$	–	–	–	–	–	0.997
2nd partitioned wave system	Hm_{0_2}	−0.017 m	0.067 m	0.133	0.97	0.943	–
	$Tp_{\_2}$	−0.126 s	1.719 s	0.175	0.92	0.846	–
	$Dm_{\_2}$	–	–	–	–	–	0.971
3rd partitioned wave system	Hm_{0_3}	−0.014 m	0.104 m	0.330	0.85	0.720	–
	$Tp_{\_3}$	−0.117 s	1.833 s	0.203	0.94	0.878	–
	$Dm_{\_3}$	–	–	–	–	–	0.928

analysis between numerically reconstructed spectra and their corresponding initial forcing spectra is intended to evaluate and validate the correct performance of the directional analysis and spectral reconstruction method. The BIAS deviation, root mean square error (RMSE), bisector dispersion (Scatter Index, SI), bisector correlation (CORR), and correlation coefficient (R^2) have been used to evaluate the performance in terms of scalar parameters (wave height and period parameters). The circular correlation coefficient (Rc; Jammalamadaka and SenGupta, 2001; NCSS, 2022) has been used to measure the correlation between circular variables (wave direction parameters). The main statistical and correlation coefficients obtained from the comparison in terms of aggregated and separate spectral parameterization for each of the three main wave systems from directional spectra partitioning are summarized in Table 1. The spectral partitioning has been performed by means of the open-source library code Wavespectra (GitHub – metocean/wavespectra, MetOcean Solutions Ltd., 2018). This code provides a spectral tool for directional spectra partitioning based on the watershed algorithm (Hanson et al., 2009).

Highly correlated results (Table 1) are obtained from the comparison of both aggregated and partitioned spectral wave characteristics between initial forcing spectra (previously obtained from SWAN modeling) and those numerically reconstructed near the wave generation contour in the numerical domain in MSPv2.0 after performing the monochromatic-based numerical transformation and spectral reconstruction. Most of the inaccuracy in evaluating statistical coefficients for separated wave parameter estimations arises due to the parameter-based comparison. In the partitioning step, small curvature deviations in the spectral wave energy surface can result in different separate partitions. That is, a single peak in an original forcing spectrum can be divided into two separate peaks, with the same frequency and separated in direction or, conversely, the same direction and different frequency, in the reconstructed spectrum, and vice versa.

Additionally, a visual comparison between the initial and reconstructed spectra in terms of the complete spectral shape is presented in Fig. 5. The numerically obtained spectrum, as well as its corresponding forcing spectrum, for three sample sea states with different n-peaked (unimodal, bimodal and trimodal) directional spectra are represented. Good performance of the method is observed for the three different spectral shapes. As can be seen, very similar frequency-direction wave energy distributions are obtained for the numerically reconstructed spectra compared to the initial forcing spectra. All wave components, with different frequencies and directions, are consistently estimated. Aggregated and partitioned spectral wave parameters are also indicated in Fig. 5. Analogous values between baseline and estimations, for both aggregated and partitioned spectral parameters, are obtained for all different spectral shapes.

After the previous validation based on the outer-port forcing spectra reconstruction, a validation of the method for in-port directional spectra reconstruction has been performed. The validation of the method applied at the AWAC position deployed inside the port basin (point A7; Fig. 1b) has been performed for 1 month of available measured data. A comparison of spectral wave parameters obtained from numerically reconstructed spectra with those from instrumental data is shown in Fig. 6a. The statistical coefficients assessing the goodness of fit for each different parameter are also indicated. An adequate estimation in terms of aggregated spectral parameters is presented, especially for Hm_0 and Tm_{02}. Larger deviations are observed in terms of aggregated Tp (Fig. 6a). However, as can be seen in Fig. 6b, higher correlation coefficients are obtained if the partitioned peak period of one of the two main separate wave systems ($Tp_{\_1}$ or $Tp_{\_2}$) is considered instead in the analysis. More uniform values in a narrower directional range are observed for wave direction estimations compared to instrumental data (Fig. 6a). This lower directional variability may be because only 1 month of instrumental data is available. Indeed, this statistically limited directional variability is also observed in the time series of the aggregated Dm of the initial forcing spectra (Fig. 6c). Unimodal outer-port spectra coming from the NNE are registered for all the hourly sea states during the entire covered month of analysis.

Taking the advantage of the available measured directional wave spectral information, a comparison of numerically reconstructed directional spectra with those from postprocessing the AWAC instrumental data has also been performed. It is worth mentioning the scarcity of existing works in the literature dealing with directional wave measurement in harbors. Some applications of AWACs deployed within ports, although not for the directional spectrum estimation, can be found in Guo et al. (2021), Shih (2012), and Zheng et al. (2020, 2022). This comparative analysis is intended to evaluate the performance of the proposed numerical method compared to this other existing AWAC measurement-based method to estimate the directional wave spectrum. However, it is important to note the difference of approach between the presented numerical methodology and that followed in the postprocessing of the AWAC measured information. In this latter, a widely used DSF-based expression is adopted to calculate the directional wave spectrum. The Maximum Likelihood Method with Surface Tracking (MLMST) is the postprocessing method used to estimate the directional wave energy distribution from AWAC measurements (Nortek, 2017).

A sample comparison between numerically reconstructed and AWAC-postprocessed directional wave spectra is presented in Fig. 7. From the analysis of these numerical and instrumental-based directional spectra, the well-resolved multimodality of waves (expected for in-port wave fields) can be observed in the numerical wave agitation spectra obtained with the proposed methodology. Different incoming, diffracted

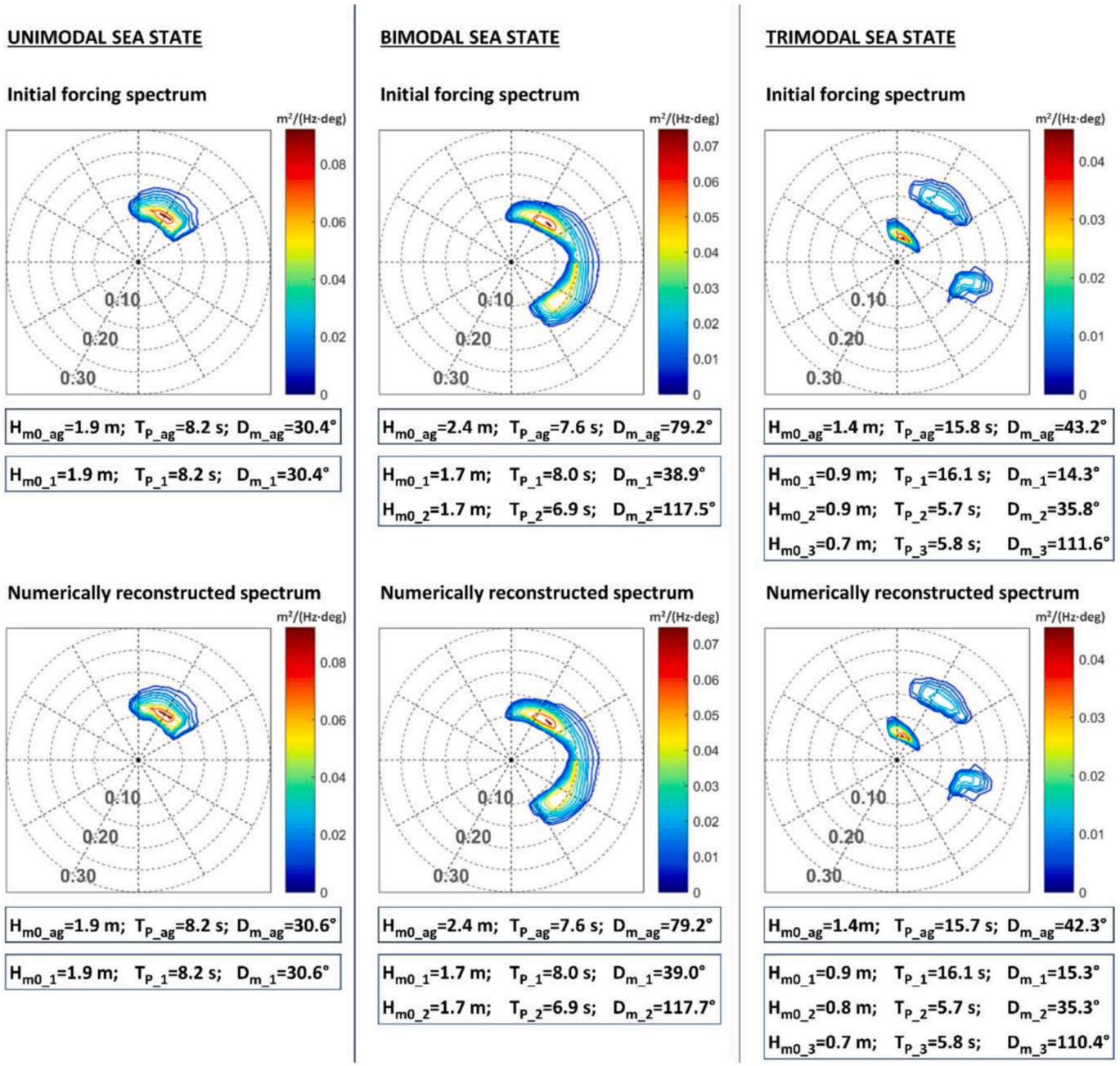

Fig. 5. Validation of the method for directional spectra reconstruction (frequency-direction space). Comparison of numerically reconstructed directional spectra (bottom), near the wave generation contour in the MSPv2.0 model, with the corresponding initial forcing spectra (top), for different n-peaked (n = 1, 2 and 3) spectral shapes. Aggregated and partitioned spectral parameterization.

and reflected wave systems are clearly separately represented in multipeaked numerically reconstructed spectra. With respect to the post-processed instrumental information, considerably wider and combined directional spectral shapes are presented for AWAC spectra. This could be expected since smoother-peaked and broader directional spreading functions are usually estimated by the MLM method (Benoit, 1994; Benoit et al., 1997; Donelan et al., 2015; Pascal and Bryden, 2011), especially for multimodal waves. In addition, limitations of the MLM to identify and separate the incident and reflected waves due to a phase correlation (Frigaard and Andersen, 2014; Huntley and Davidson, 1998) should be kept in mind. Narrower directional distributions in numerically reconstructed spectra can result since directional spreading is not explicitly solved. The main direction of each monochromatic wave subsystem is estimated. The spreading in agitation spectra arises from the contribution of each subcomponent to each pair frequency-direction. Some deviated subcomponents can be included in highly multidirectional waves, since true and fictitious energy can be confused in r-DPRA analysis. However, the fine discretization, both in frequency and direction, adopted for the spectral reconstruction approach allows minimization of the effect of such deviations in the total reconstructed spectra. Finally, both the MLM and r-DPRA methods are sensitive to gauge and mesh node configurations, respectively (Benoit, 1994; de Jong and Borsboom, 2012; Nortek, 2017; Van Essen et al., 2013). Therefore, the aforementioned behavior of narrower directional wave energy distributions in numerically predicted spectra compared to instrumental data-based (Fig. 6) could be explained by all these approach differences. Nevertheless, despite the limitations/assumptions of each method mentioned above, similar behavior of wave

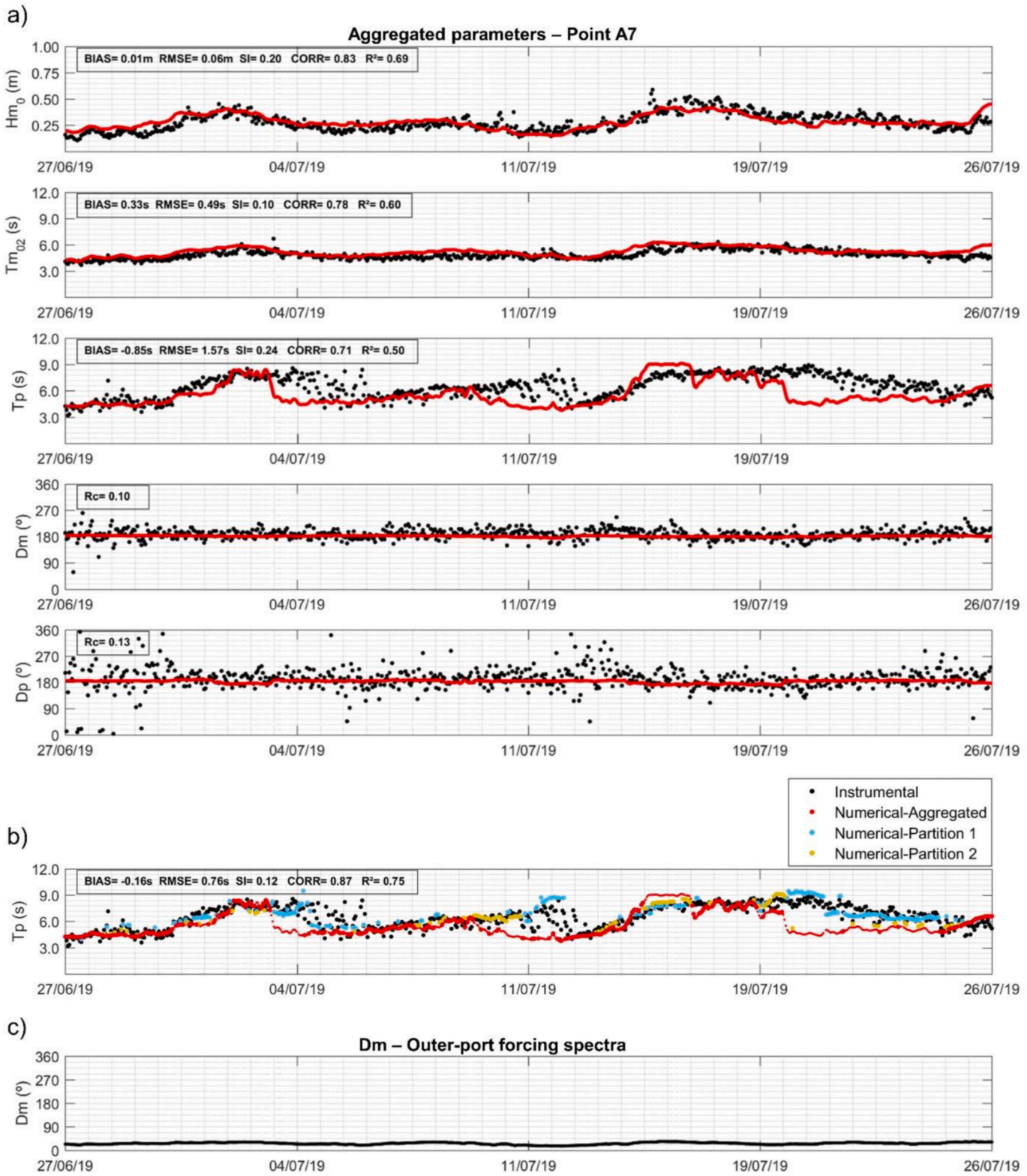

Fig. 6. a) Time series of aggregated spectral parameters at control point A7 (AWAC, 1 month). Instrumental data (black points), numerical results (red line). Statistical fit and correlation coefficients. b) Time series of separate Tp_{-1} and Tp_{-2}, from spectral partitioning, in addition to aggregated Tp from numerically reconstructed spectra; aggregated Tp parameter from AWAC instrumental data. c) Time series of Dm in the outer-port forcing spectra. Visualization of the low variability of wave direction, Dm parameter, for all the hourly forcing unimodal spectral shapes coming from the NNE sector.

directionality can be appreciated for differently sourced data-based spectra, thus validating the proposed numerical methodology and highlighting its ability to resolve multimodality of spectral in-port wave agitation. For example, the reflected waves coming from the Reina Sofia breakwater, with SSW wave directions, are distinguished from the diffracted waves (SSE directions) around the Nelson Mandela breakwater at the port entrance in the numerically reconstructed spectra. Single broader wave components, with peak direction from the SSW, and

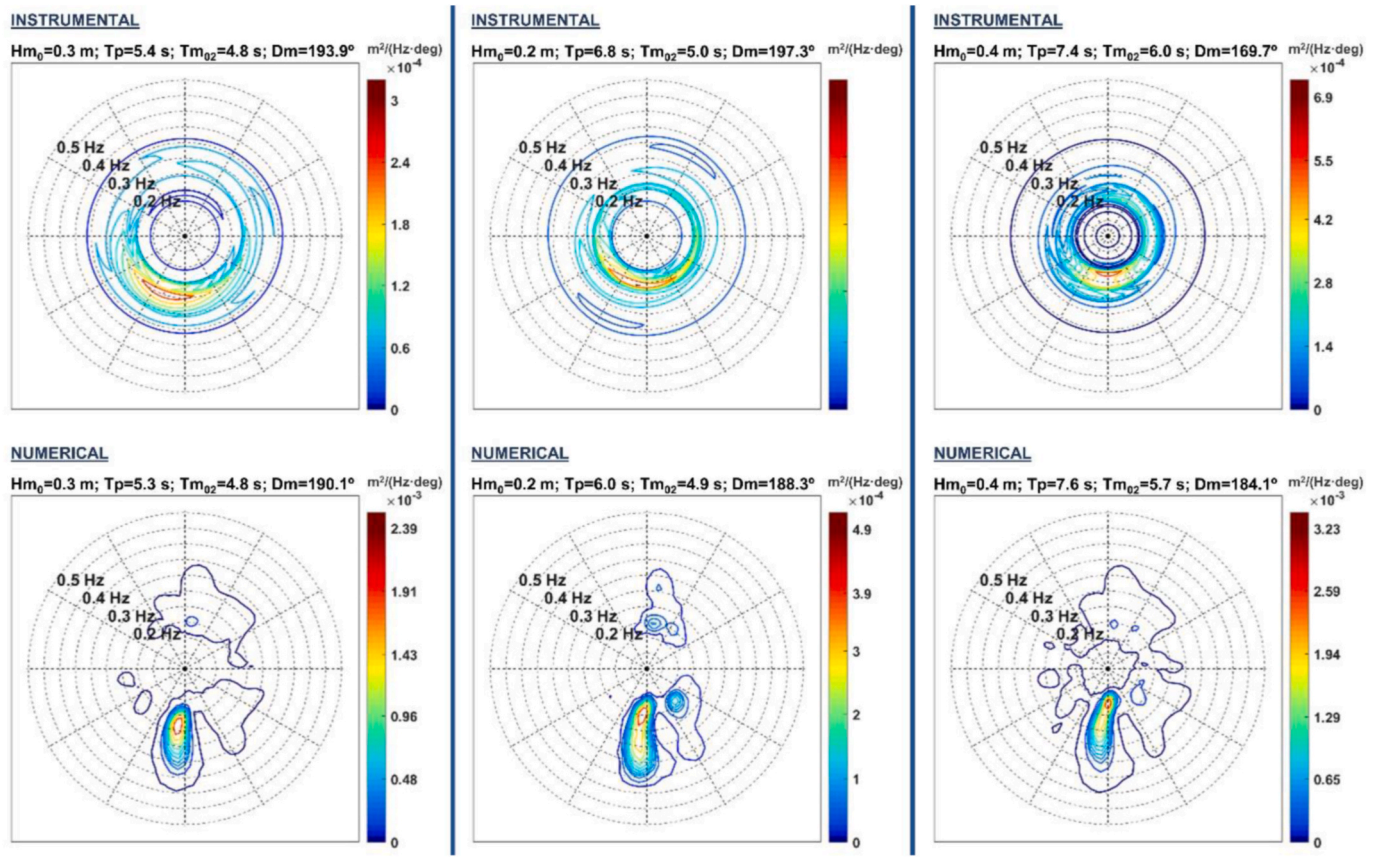

Fig. 7. Comparison of numerically reconstructed directional spectra with instrumental data-based directional spectra from the postprocessing of AWAC information for different spectral shapes.

directional spreading covering the directional ranges of such separated wave systems are present in the AWAC spectra. In those cases where the diffracted waves acquire more relevance in the numerical spectra, the wave energy in the AWAC spectra is slightly displaced to the SSE direction.

Finally, the directional spectra reconstruction has also been applied and validated at the positions of the wave agitation sensors (points D1-D6 in Fig. 1b). Directional measured information is not available at these positions, so a comparison between numerical and instrumental scalar wave parameters has been performed for validation. Comparison of the Hm_0, Tm_{02} and Tp time series at points D2 and D4 are shown in Figs. 8 and 9, respectively.

From the analysis of the parameter-based comparison between numerically predicted wave agitation information and that from the field campaign, adequate goodness of fit is obtained in terms of scalar aggregated wave parameters at all the analysis positions. As previously seen in the validation at point A7, increased correlation and quality of fit are obtained for the Tp parameter if separate Tp_1 and Tp_2 are considered in the analysis. Higher evaluating coefficients are presented in the Tp series in Figs. 8b and 9b compared to those from Figs. 8a and 9a, respectively.

3.4. Spectral types (ST) definition (D)

In this last step of the methodology, from historical series of wave agitation spectra, ST clustering is performed to identify the representative spectral patterns of wave agitation within any harbor. In this way, the complete statistics of the historical wave agitation climate are compactly gathered into a reduced number of representative STs, each with an associated probability of occurrence.

ST clustering is achieved by means of a 2-substep multivariate statistical downscaling, adopting a similar approach to that proposed in Camus et al. (2014) for sea level pressure-based weather type definition. A first data dimensionality reduction is performed prior to the clustering of the database into representative patterns.

The historical hourly discretized directional spectra have been previously generated at each of the 7 control points by following the dynamic approach described in Section 3.3. Due to the high dimensionality of the generated spectral database, prior to the clustering algorithm application, a reduction of dimensionality is carried out by performing a Principal Component Analysis (PCA). In this way, the historical discretized spectra at each of the 7 basin positions have been projected to a new space, defined by Empirical Orthogonal Functions (EOFs), and their corresponding amplitudes by Principal Components (PCs). The dimensionally reduced definition is achieved with a limited number of selected components required to maintain a predefined percentage of variance. A dimensionality reduction of almost two orders of magnitude has been achieved, in this case, for a 99% explanation of variance.

The clustering algorithm has subsequently been applied to each of those PCs series. Different clustering and selection methods are presented in Camus et al. (2011), dealing with time series of typical sets of 3-parameter spectral wave definition (Hm_0, Tp and Dm). From all those described, the K-means algorithm (KMA) is concluded to be the most appropriate for average wave climate characterization. This algorithm allows clustering the historical hourly 3-parameter sea states into a reduced number of representative cases. An iterative clustering procedure is performed based on the grouping of each dataset to the nearest cluster in a Euclidean space. The centroid of each cluster is updated at each iteration step. In this work, the abovementioned trivariate KMA algorithm has been used for ST clustering, adapting it to deal with a frequency-direction multivariate space. Instead of a random initialization, the initial centroids are defined by a previous application of the

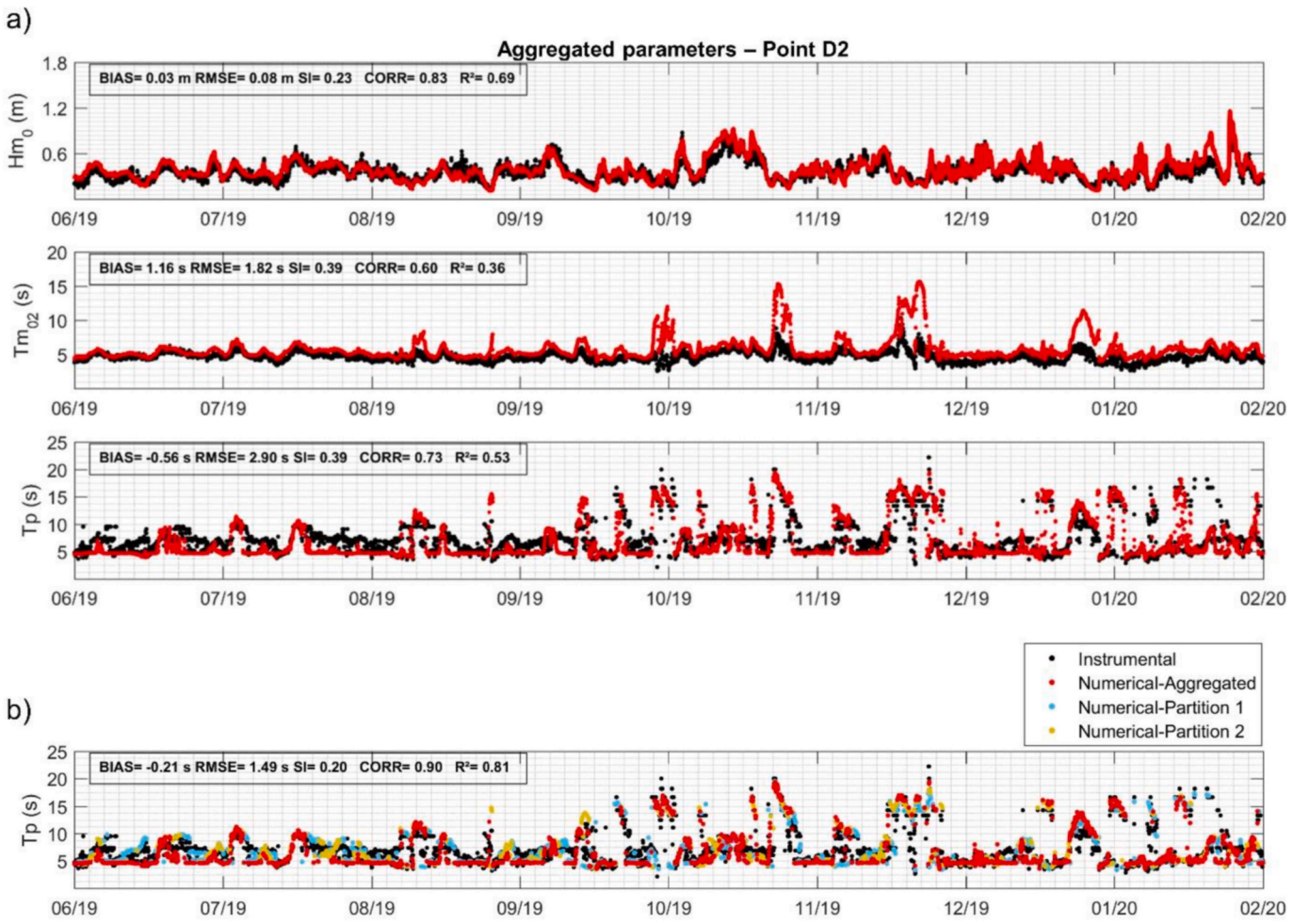

Fig. 8. a) Time series of aggregated spectral parameters at control point D2 (8 months). Instrumental data (black points), numerical results (red points). Statistical fit and correlation coefficients. b) Time series of separate main, T_{P_1}, and secondary, T_{P_2}, from spectral partitioning, in addition to numerical and instrumental-based aggregated Tp parameter.

maximum dissimilarity algorithm (MDA) (Camus et al., 2011) to pre-select more spatially dispersed data (Camus et al., 2014). Last, the centroids of the final clusters are projected in reverse from the EOF space to the original frequency-direction space, resulting in an ST representation of the long-term wave agitation climate at each inner position analyzed.

The number of STs established in the clustering procedure has been assumed to be enough to achieve an adequate description of the historical time series but not excessive to hinder the clear interpretation. The more STs there are, the more refined the clustering will be but also the more burdensome to interpret/visualize. With the aim of defining the appropriate number of cases in this work, a sensitivity analysis has been carried out for different square lattice sizes, from 3 × 3 to 10 × 10 spectral types. Two evaluating coefficients have been used to assess the results for different sizes of clustering at each of the 7 control points. The reduction involved in the average distance from each hourly spectral dataset in the historical time series to its corresponding representative pattern (centroid of cluster) is represented in Fig. 10a. The proportion of variance explained (EV; Eq. (2)) (Camus et al., 2016; Cannon, 2012) is represented in Fig. 10b. Both performance indicators can be interpreted as a measure of the dispersion of data within clusters to evaluate the refinement achieved with larger lattices.

$$EV = 1 - \frac{SSE}{SSE_T} \tag{2}$$

where SSE is the within-cluster sum of squared error from each dataset to its representative centroid, and SSE_T is the total sum of squared errors of the historical dataset.

The decreasing trend of the average distance from datasets to each centroid, while increasing the EV coefficient, as the number of clusters increases in the clustering procedure, can be observed in Fig. 10. From the ST lattice size of 5 × 5, a mean dataset-centroid average distance reduction below 8%, as well as an EV coefficient higher than 70%, are obtained. For larger lattices, excessive clustering is observed since the mean probability of occurrence of the least probable spectral type decreases to 0.2 h/year, which means that clusters with only one hourly data from the 40-year historical series are obtained from the clustering procedure at some control positions. In addition, a more complicated interpretation is provided by larger ST lattices. Therefore, a lattice of 5 × 5 spectral types is proposed for the historical spectral wave agitation climate characterization in this work.

4. Results and discussion

In this section, the obtained results from the proposed methodology applied in Africa basin are presented. An improved harbor agitation climate characterization, based on the interpretation of the representative STs obtained at the different control points, is performed. A comprehensive and disaggregated description of the multiple wave transformation processes comprising the multidirectional spectral wave agitation maps is presented. The improvement achieved with this new directional spectral approach compared to usual aggregated Hm_0-based

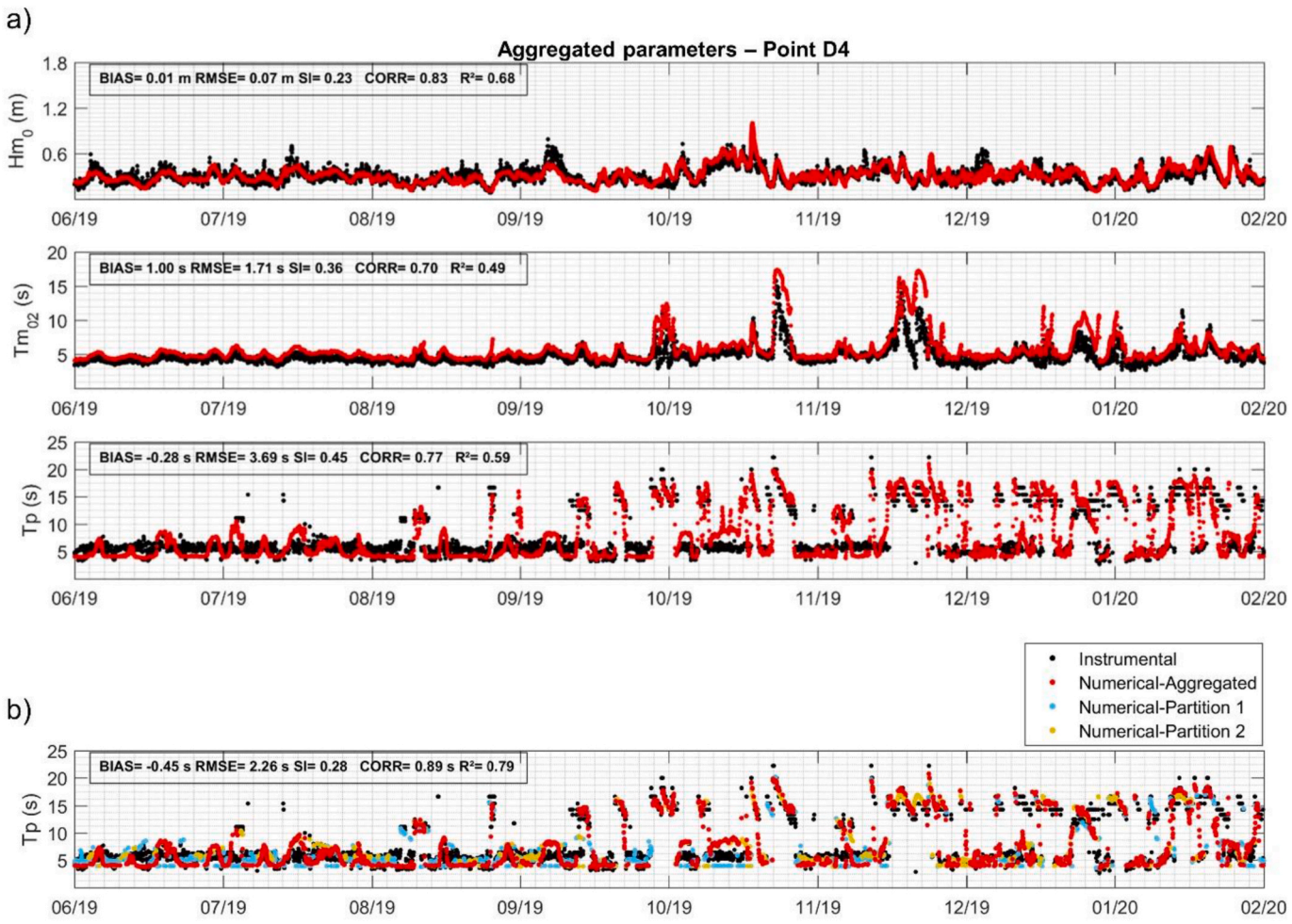

Fig. 9. a) Time series of aggregated spectral parameters at control point D4 (8 months). Instrumental data (black points), numerical results (red points). Statistical fit and correlation coefficients. b) Time series of separate main, T_{P_1}, and secondary, T_{P_2}, from spectral partitioning, in addition to numerical and instrumental-based aggregated Tp parameter.

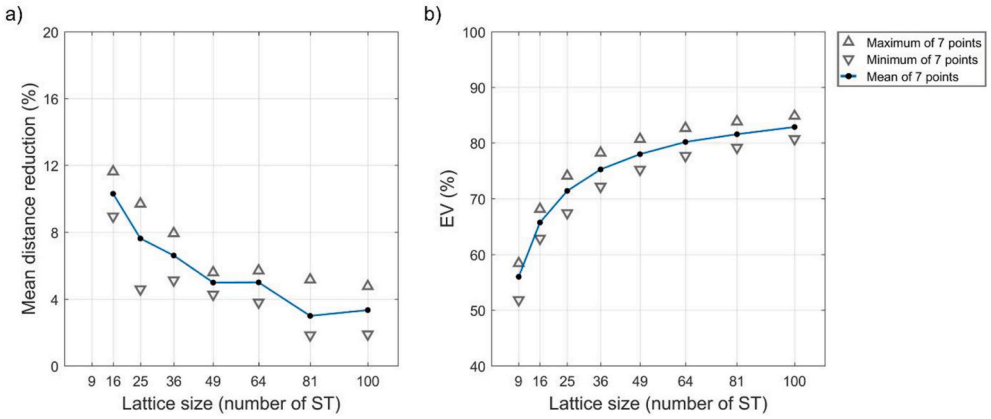

Fig. 10. Performance assessment of the clustering procedure for different sizes of clustering. a) Reduction (%) involved in the mean distance from each historical dataset to their representative pattern (centroid of cluster); b) Proportion of variance explained, EV (%).

approaches for wave agitation characterization is demonstrated.

Lattices of 5 × 5 wave agitation spectral types have been elaborated at all the control positions (D1-D6, A7; Fig. 1b). However, for the sake of brevity in this article, reduced lattices with the most relevant wave agitation STs at the different control points are presented. For the current analysis, the STs in lattices have been represented by order of similarity while keeping ST1 and ST2 for the most energetic and most frequent wave agitation ST, respectively, at each control position. In order to assess the spatially variable wave agitation response of the study basin in relation to the outer-port wave climate, the outer-port forcing spectra associated with each in-port ST are also represented. In addition to the spectral shape pattern, the information associated with

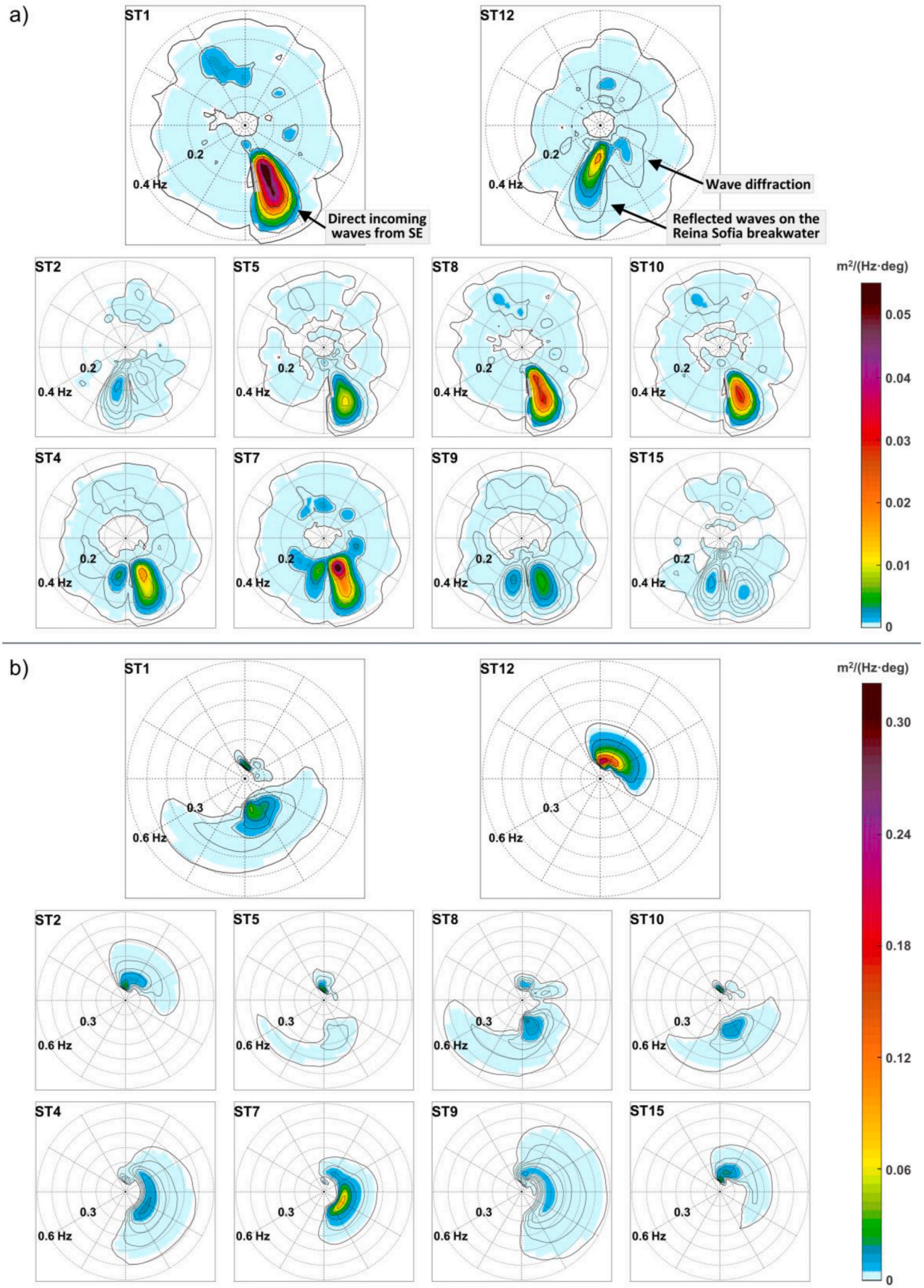

Fig. 11. Point A7. Summary of the relevant information for the visualization of the different processes of the wave energy penetrating into the study port basin. a) Wave agitation spectral types (ST, m^2/Hz·deg); b) Outer-port spectra corresponding to each wave agitation spectral type (ST, m^2/Hz·deg).

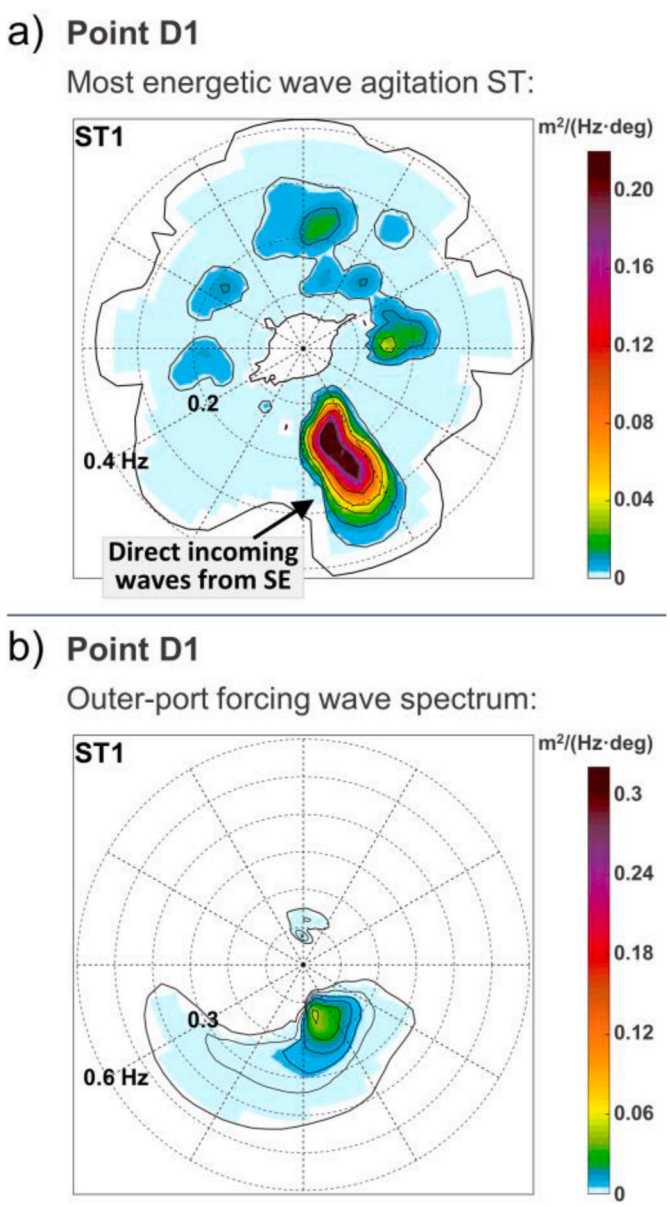

Fig. 12. Point D1. a) Most energetic wave agitation ST. b) Outer-port forcing spectrum corresponding to the wave agitation ST.

all the historical sea states it represents is effectively gathered in each representative ST. In this way, a statistical characterization of the long-term in-port wave agitation in terms of Hm_0 is performed in this analysis.

From the analysis of the local results obtained at the control positions, a clear description of the outer-port spectral wave transformation according to the geometry and structural typologies of port contours is achieved as follows.

First, from in-port ST-based characterization at point A7, located in the middle of the port basin (Fig. 1b), an interesting visualization of the different processes of the wave energy penetrating into the port basin is obtained, which is an essential initial step for any harbor wave climate assessment. The relevant information for this analysis at point A7 is summarized in Fig. 11. The wave agitation STs at point A7 are presented in Fig. 11a. The outer-port forcing spectra associated with each in-port spectral type are represented in Fig. 11b. From these results, three main processes of wave energy penetrating into the basin are identified: (1) direct incoming waves from SE directions (e.g., ST1 in Fig. 11a), (2) wave diffraction around the end of the Nelson Mandela breakwater, and (3) inward projection by wave reflection on the Reina Sofia breakwater. These two latter processes can be appreciated, for example, in ST12 (Fig. 11a), where two different in-port wave components are clearly observed: firstly, the in-port SE wave component resulting from the wave diffraction process at the port entrance and, secondly, the in-port SSW wave component corresponding to the wave energy reflected on the exterior Reina Sofia breakwater. Both in-port wave components result from a unimodal forcing spectrum with a single NE wave energy component.

Due to the south orientation of the port entrance, Africa basin is unfavorably exposed to outer-port waves coming from SE-SSE directions. These waves directly impact the western area of the basin, as can be clearly seen in ST1 (i.e., the most energetic ST), ST5, ST8 and ST10 at point A7 (Fig. 11a and b). Indeed, outer-port waves from the SE-SSE are the most adverse wave conditions for in-port wave agitation at the western half of the basin. As can be seen in Fig. 12, the highest wave agitation levels at point D1 (Fig. 12) correspond to a forcing spectrum with the main wave energy component coming from the SSE.

Outer-port SE waves, after penetrating into the western half of the basin, are then reflected to the rest of the port basin. For example, these reflected waves can be appreciated (Fig. 13) in ST4 at point D5 (located on the opposite eastern side of the basin) and ST1 at point D6 (located in the southern-lee side of the main breakwater). In such spectra, the increased relative wave energy coming from western directions is observed while this in-port reflected wave energy disappear in the narrower ST24 at point D5 (Fig. 13), driven by an outer-port forcing spectrum with its main wave energy coming from N direction.

A statistical characterization of the long-term in-port wave agitation climate, in terms of Hm_0, associated with the different STs at point A7 is presented in Fig. 14. The intra-ST probability of occurrence (between 0 and 1) according to different ranges of Hm_0 values is represented by the stacked bar chart. The annual probability of occurrence of each ST is indicated at the top of each bar. That is, the Hm_0 absolute probability of occurrence corresponds to the intra-ST probability of occurrence, conditioned to the corresponding annual probability of occurrence of each ST. Hm_0 values are represented by a color scale, from dark red to green color for the highest to lowest Hm_0 values, respectively.

In Fig. 14, the outer-port SE spectral shapes (ST1, ST5, ST8 and ST10) are not the most frequent wave climate conditions; they present a cumulative annual probability of occurrence around 1.3% (i.e., 114 h per average year; Fig. 14). However, these SE wave components can also be relevant for in-port wave agitation when they appear combined with other wave directions in multimodal or in widely spread wave energy spectra such as ST4, ST7, ST9 and ST15 (Fig. 11b), which present a cumulative annual probability of occurrence around 8.5% (i.e., 745 h per average year; Fig. 14). Indeed, from the analysis of the long-term statistics of in-port wave agitation Hm_0 at control point A7 (Fig. 14), the five highest wave agitation levels are identify for ST1, ST7, ST8, ST10 and ST4, in decreasing order. That is, two STs in the top 5 of the most energetic wave agitation STs at point A7 correspond to these widely spread wave energy spectra: ST7 (rank 2) and ST4 (rank 5). On the other hand, low wave agitation levels are observed for the most frequent ST (ST2). This illustrates the importance of using the ST-based characterization for a highly multimodal outer-port wave climate.

The most energetic ST at points D3, D4 and D5 are presented in Fig. 15. As can be seen, the most energetic in-port spectral types in the eastern half of the basin are associated with unimodal-shaped outer-port wave spectra coming from the NNE, with intermediate peak periods, and shorter-period spectral components spread to eastern directions. The study basin is not directly exposed to these northern wave climate conditions but these waves are projected toward the north and eastern zones of the basin after reflection on the Reina Sofia breakwater, driving to the highest wave agitation levels in such zones. For the similar outer-port forcing wave conditions, the different in-port wave agitation spectra at each control point can be analyzed providing a comprehensive visualization of the spatial variability of wave agitation within Africa

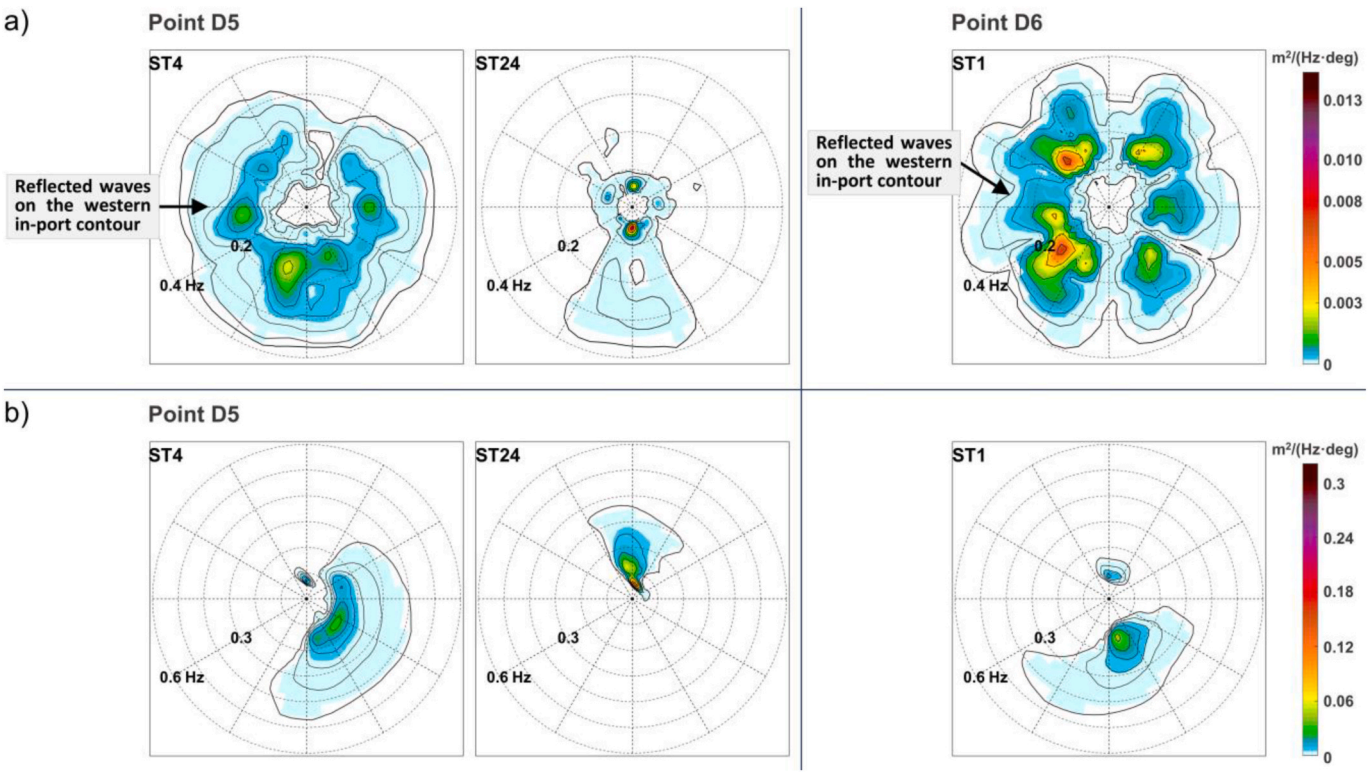

Fig. 13. Points D5 and D6. a) Wave agitation ST: ST4 and ST24 at point D5; ST1 (i.e., the most energetic ST) at point D6. b) Outer-port forcing spectra corresponding to each wave agitation ST.

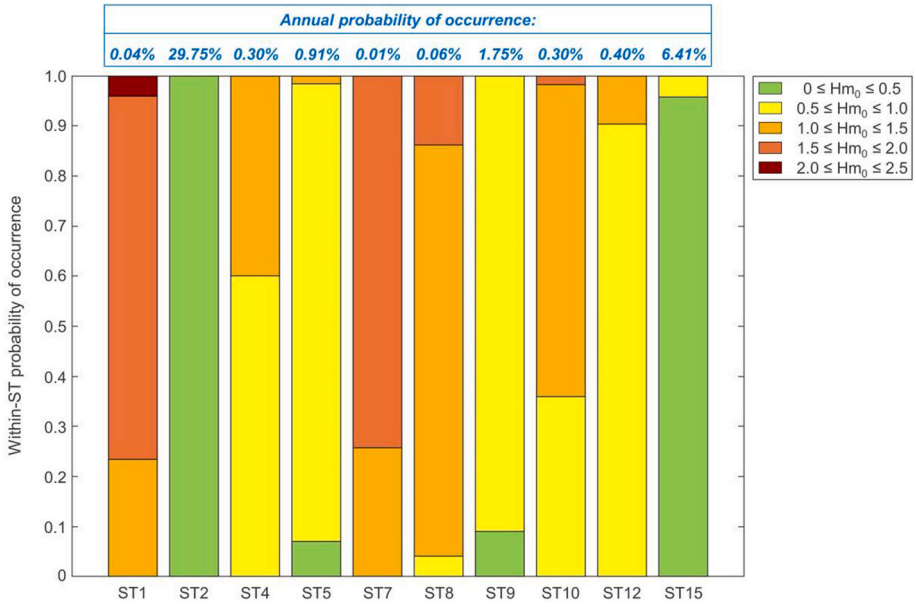

Fig. 14. Long-term statistics of the in-port wave agitation climate, in terms of Hm_0, associated with different STs at point A7. Stacked bar chart of the intra-ST probability of occurrence of different Hm_0 values. Annual probability of occurrence (%) indicated above the bar chart. Hm_0 ranges represented by a color scale.

basin.

In this way, from the analysis of different ST shown in Fig. 15, a higher influence of shorter periods (frequency $\geq$ 0.15 Hz) is observed at point D5. A characteristic wave agitation pattern of dominant in-port wave systems practically parallel to the wall can be identified at that point. The main affection of intermediate periods (0.10 $\leq$ frequency $\leq$ 0.15 Hz) in the north part of the basin (point D3) can be observed from STs in Fig. 15. Finally, as might be expected, the highest spectral peak at point D4 (which is located near a corner in the basin) corresponds to longer periods (frequency $<$ 0.1 Hz).

As presented in Section 3.1, outer-port mean wave directions coming from NNE, with Tp between 5 and 10 s, are the predominant wave system conditions to which Africa basin is exposed. Accordingly, the most frequent in-port spectral types (with annual probabilities of occurrence between 25% and 30%) at all the control points are associated with such spectral wave characteristics. The ST2 at point A7

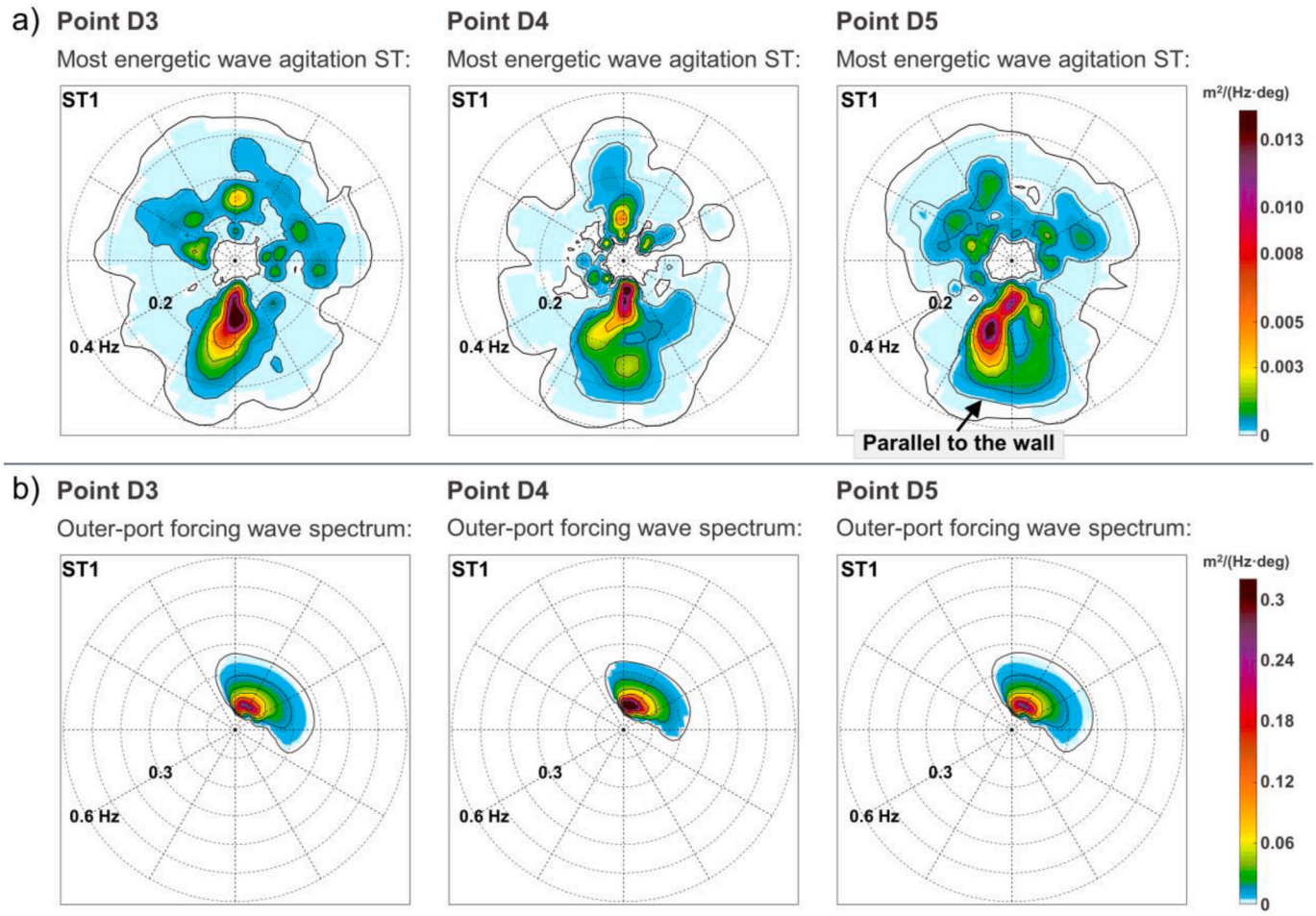

Fig. 15. Points D3, D4 and D5. a) Most energetic wave agitation ST at points D3, D4 and D5. b) Outer-port forcing spectra corresponding to each wave agitation ST.

(29.75% of probability of occurrence) can be visualized in Fig. 11. For the current analysis, the most frequent STs at points D3, D4 and D5 are analyzed. They are driven by the same forcing spectrum (Fig. 16a). It is a bimodal spectral shape, with the main component coming from the NNE with an intermediate peak period and a secondary northern component with a longer peak period. Specifically, it can be defined by the following set of parameters: ($H_{m0\_1} = 1.2$ m, $T_{P\_1} = 7.5$ s, $D_{m\_1} = 25.0°$; $H_{m0\_2} = 0.4$ m, $T_{P\_2} = 11.3$ s, $D_{m\_2} = 1.3°$). It presents a 28.1% of mean annual probability of occurrence, with seasonal probabilities of occurrence of 13.9% (December–February), 24.5% (March–May), 42.9% (June–August) and 30.8% (September–November). The predominance of outer-port waves from the NNE, with a lower variability for summer months (June–August), stands out. This is consistent with that observed in Section 3.3 from AWAC data analysis.

The corresponding agitation map for the outer-port forcing spectrum inducing the most frequent ST at points D3, D4 and D5 is also presented in Fig. 16b. An aggregated visualization of the wave agitation response is provided by this spectral wave agitation map where the wave energy penetrating toward the eastern area of the basin, after reflection on the Reina Sofia breakwater, can be appreciated. However, the most influential outer-port wave energy components on the in-port wave agitation at different control positions cannot be identified, as can be done from representative STs. From the analysis of STs in Fig. 16c, the main influence of the intermediate period-wave components coming from northern directions at point D3 is observed. A higher influence of shorter periods, from more eastern directions, is observed at points D5 and D4. This latter is impacted by the aforementioned locally generated wave systems parallel to the wall.

As a summary from the analysis, it should be noted that a detailed and relevant description of the spatially variable wave agitation response is achieved by the interpretation of the representative STs at different positions within the basin. A comprehensive and disaggregated definition of the multiple wave transformation processes comprising the multidirectional spectral wave agitation maps is obtained, which is an important advance from the aggregated visualization of the wave agitation response provided by the classical wave agitation maps.

In addition, the final improvement achieved in wave agitation characterization with this new ST-based approach compared to the commonly used approaches based on aggregated Hm_0 is clearly shown by the analysis of the results obtained at point D2 (Fig. 17). The two most energetic wave agitation STs are identified for ST1 and ST5 at point D2 (Fig. 17c). Both spectral types present similar long-term statistics of the in-port wave agitation climate, in terms of the spectral-aggregated Hm_0, where the influence of each different wave system on the wave agitation response is masked in a total value of wave height. However, very different spectral shapes are identified in terms of both in-port wave agitation (Fig. 17a) and outer-port forcing (Fig. 17b) spectra. This demonstrates the improvement achieved with this new directional spectral approach compared to usual aggregated Hm_0-based approaches for wave agitation characterization.

To conclude, the local representative patterns, in terms of aggregated spectral parameters (Hm_0, Tp and Dm) of the historical wave agitation climate at each control position obtained from the multidimensional spectral clustering, are represented in Fig. 18. The different multivariate patterns identified from the multidimensional-space-based clustering can be observed, which cannot be achieved through a single-parameter-

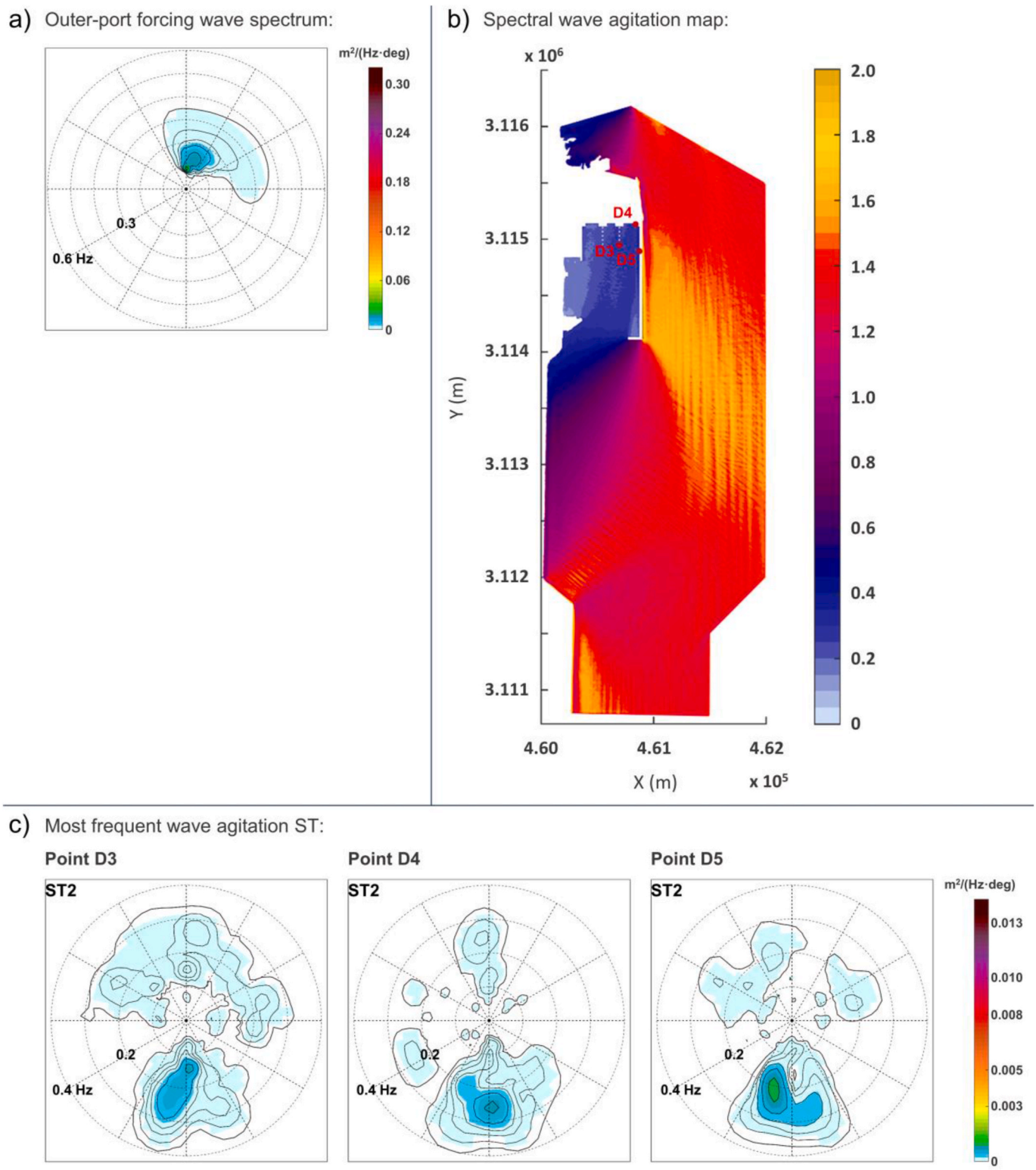

Fig. 16. a) Outer-port forcing spectrum corresponding to the most frequent wave agitation ST at points D3, D4 and D5. b) Corresponding spectral wave agitation map. Visualization of wave propagation over the entire numerical domain defined in MSPv2.0; position of control points D3, D4 and D5. c) Wave agitation ST2 at D3, D4 and D5.

based approach. For example, clearly different groups of trivariate datasets can be visualized in Fig. 18 for ST1 (blue color) and ST5 (red color) at point D2, in contrast to the similar long-term statistics of the in-port wave agitation climate, in terms of the spectral-aggregated Hm_0, observed in Fig. 17c.

5. Conclusions

A new methodology for improved wave agitation climate characterization based on a representative frequency-direction wave spectrum definition within harbors has been presented in this work. An in-depth

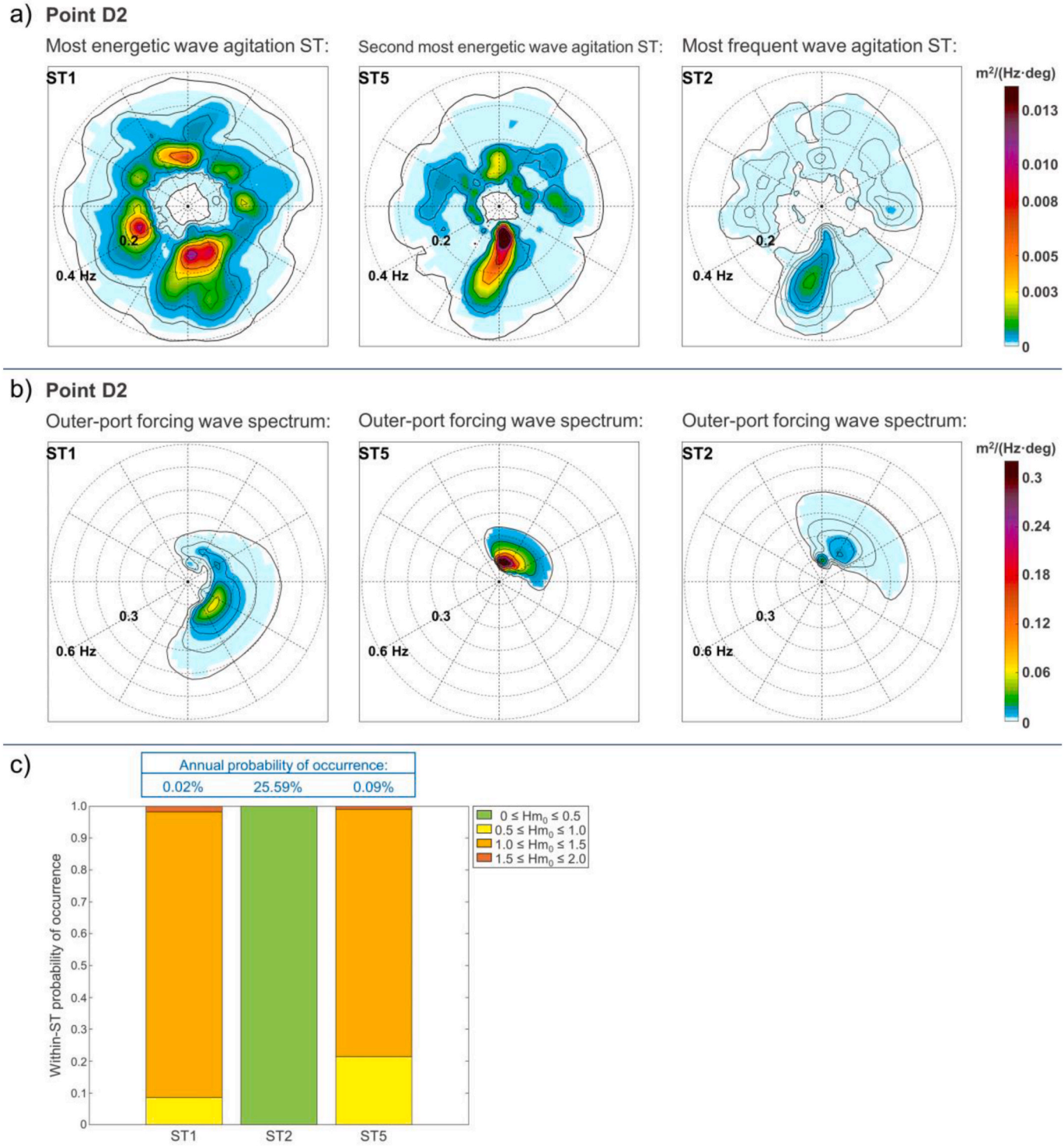

Fig. 17. a) ST1: Most energetic wave agitation ST at point D2. ST5: Special case; Second most energetic wave agitation ST at point D2. ST2: Most frequent wave agitation ST at point D2. b) Outer-port forcing spectra corresponding to each agitation spectral type. c) Long-term statistics of the in-port wave agitation climate, in terms of Hm_0, associated with different STs at point A7.

description of the whole multidirectional and multireflective wave patterns occurring as a harbor wave agitation response, related to the outer-harbor wave climate, is achieved.

The complete numerical methodology has been described, applied and validated in Africa basin located in Las Palmas Port (Spain). A dynamic spectral wave downscaling approach has been followed. A disaggregated frequency-direction wave spectra definition of the hourly historical wave agitation patterns, at any position inside the harbor, has been achieved. Then, a statistical assimilation of those historical time series of directional wave agitation spectra has been performed based on a clustering method of representative spectral types (ST). In this way, the long-term and spatially variable wave agitation climate within the port basin is efficiently characterized by a reduced number of characteristic local wave agitation STs (each with an associated probability of occurrence).

Complex aggregated wave agitation patterns arise in highly

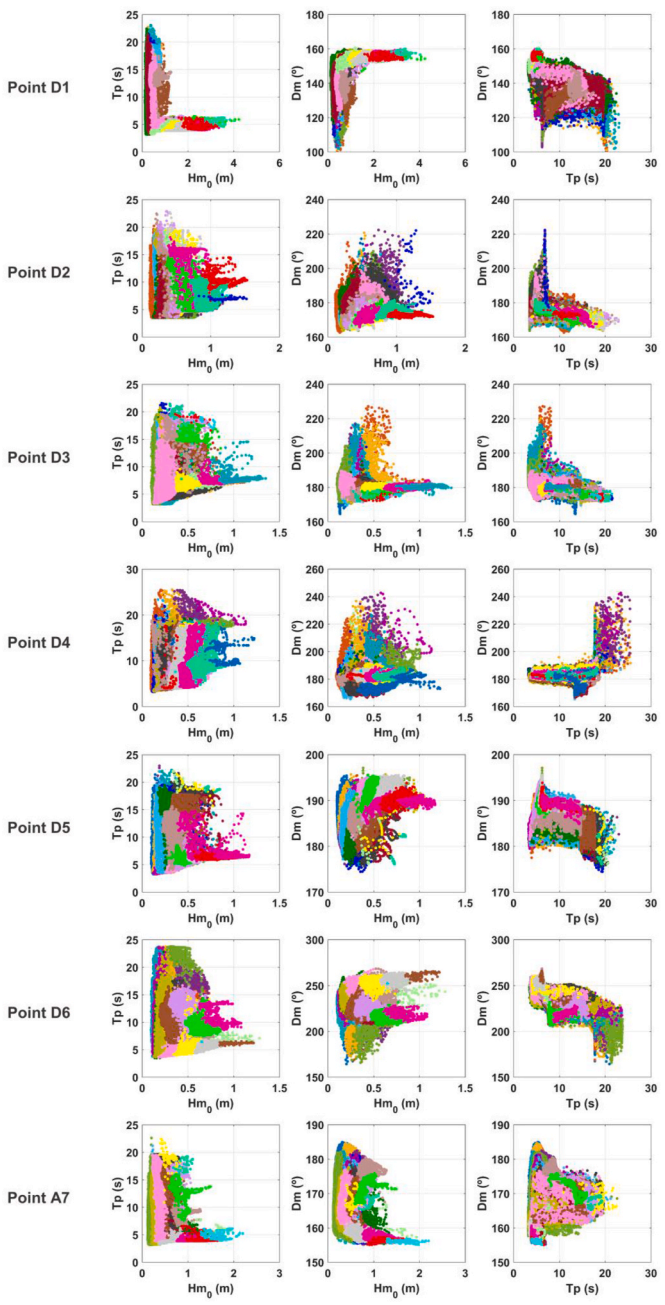

Fig. 18. Aggregated parameters (Hm_0, Tp, Dm) of the historical wave agitation directional spectra at each control position grouped into 5 × 5 corresponding clusters. Datasets in different clusters are represented by different colors. 2D projections of the 3D (Hm_0, Tp, Dm) space.

multimodal wave climates such as that of the current study. From the ST-based wave agitation climate characterization, a comprehensive description of the historical wave agitation response related to the outer-harbor wave climate and to the multiple wave penetration and transformation processes according to the geometry and structural typologies of port structures within the port basin is attained. For example, in Africa basin, three different processes have been identified of outer-port wave energy penetrating into the basin and differently affecting the in-port/berthing control areas. The most influential wave energy components on the in-port wave agitation at different control positions have been identified. Finally, the advancements achieved with this new ST-based approach compared to the monoparametric aggregated Hm_0-based approaches for long-term multimodal wave agitation characterization have been demonstrated. A multidimensional analysis of the characteristic in-port wave agitation patterns has been performed, which cannot be achieved through a single-parameter-based approach.

To conclude, this disaggregated characterization of multimodal wave agitation climate can represent a relevant improvement for many future practical applications in harbors where the complete spectral in-port wave energy definition is essential, such as port operability/downtime analysis in terms of both wave height and moored ship motions, ship maneuvering aid, safety control in the mooring operations at the quayside, survivability thresholds of ships, mooring lines and fenders, identification of the suitable areas for the construction and survivability of floating elements (such as those for renewable energies), or wave energy potential assessment. For harbor operability/downtime assessment, beyond the scalar magnitude of wave height, the influence of the wave energy is determined by the spectral frequency-direction wave energy distribution. In terms of wave agitation, the unfavorable wave conditions and/or structural elements for the in-port wave agitation patterns can be identified, ultimately leading to optimized solutions/designs tailored to the operational requirements existing in the different berthing areas. Furthermore, the analysis of moored ship motions, where the frequency-direction wave energy distribution plays an important role, is the final evaluating element in port operability assessment. The efficiency and safety in the development of port operations at berths are not only conditioned by the magnitude of the forcing agents inducing the moored ship response but they are highly dependent on the characteristics of the local met-ocean agents and their multidimensional interaction with the structure and the ship (MarCom Working Group, 2012; Molina-Sanchez et al., 2020). Therefore, this improved definition of the local in-port wave climate in berthing areas may result in more accurate predictions of moored ship response, either through a better (multimodal) definition of wave forcing for numerical/physical modeling approaches, or through a detailed (multivariate) description of wave climate used as predictor information in Machine Learning/Artificial Intelligence-based inference models for prediction of moored ships' motions. Ultimately, all of the above can lead to an improved characterization/prediction of port efficiency, safety and operability/downtime levels at berths.

Credit authorship contribution statement

E. Romano-Moreno: Conceptualization, Methodology, Investigation, Data curation, Resources, Formal analysis, Writing - Original draft preparation. **G. Diaz-Hernandez:** Conceptualization, Methodology, Investigation, Resources, Supervision, Writing – Critical review. **A. Tomás:** Conceptualization, Methodology, Investigation, Resources. Writing – Critical review. **J. L. Lara:** Investigation, Supervision, Funding acquisition, Writing – Critical review.

Declaration of competing interest

The authors declare that they have no known competing financial interests or personal relationships that could have appeared to influence the work reported in this paper.

Data availability

No data was used for the research described in the article.

Acknowledgments

The authors would like to thank the Port Authority of Las Palmas for their cooperation and the information provided; and the CEHINAV-UPM Research Group (ETSI de Caminos, Canales y Puertos, Universidad Politécnica de Madrid) for assistance in the interpretation of instrumental data from the field campaign.

This work was supported by a FPU (Formación de Profesorado

Universitario) grant from the Spanish Ministry of Science, Innovation and Universities to the first author (FPU18/03046).

This work was also partially funded under the State R&D Program Oriented to the Challenges of the Society (PID2020-118285RB-I00) of the Spanish Ministry of Science, Innovation and Universities.

References

Barstow, S.F., Bidlot, J.-R., Caires, S., Donelan, M.A., Drennan, W.M., 2005. D. Hauser, K. Kahma, H. Krogstad, S. Monbaliu, S. Lehner et L. Wyatt. COST Office. COST. Measuring and Analysing the Directional Spectrum of Ocean Waves, vol. 714. EUR 21367.

Beltrami, G.M., Bellotti, G., Girolamo, P. De, Sammarco, P., 2001. Treatment of wave breaking and total absorption in a mild-slope equation FEM model. J. Waterw. Port, Coast. Ocean Eng. 127 https://doi.org/10.1061/(asce)0733-950x (2001)127:5(263).

Benoit, M., 1994. Extensive Comparision of Directional Wave Analysis Methods from Gauge Array Data.

Benoit, M., Frigaard, P., Schäffer, A.H., 1997. Analyzing Multidirectional Wave Spectra: a Tentative Classification of Available Methods.

Booij, N., Ris, R.C., Holthuijsen, L.H., 1999. A third-generation wave model for coastal regions 1. Model description and validation. J. Geophys. Res. Ocean. 104, 7649–7666. https://doi.org/10.1029/98JC02622.

Borsboom, M., Doom, N., Groeneweg, J., Van Gent, M., 2000. A Boussinesq-type wave model that conserves both mass and momentum. In: Coastal Engineering 2000 - Proceedings of the 27th International Conference on Coastal Engineering. ICCE. https://doi.org/10.1061/40549(276)12, 2000.

Boukhanovsky, A.V., Lopatoukhin, L.J., Guedes Soares, C., 2007. Spectral wave climate of the north sea. Appl. Ocean Res. 29 https://doi.org/10.1016/j.apor.2007.08.004.

Brocchini, M., 2013. A reasoned overview on Boussinesq-type models: the interplay between physics, mathematics and numerics. Proc. R. Soc. A Math. Phys. Eng. Sci. https://doi.org/10.1098/rspa.2013.0496.

Camus, P., Mendez, F.J., Medina, R., Cofiño, A.S., 2011. Analysis of clustering and selection algorithms for the study of multivariate wave climate. Coast. Eng. https://doi.org/10.1016/j.coastaleng.2011.02.003.

Camus, P., Menéndez, M., Méndez, F.J., Izaguirre, C., Espejo, A., Cánovas, V., Pérez, J., Rueda, A., Losada, I.J., Medina, R., 2014. A weather-type statistical downscaling framework for ocean wave climate. J. Geophys. Res. Ocean. 119, 7389–7405. https://doi.org/10.1002/2014JC010141.

Camus, P., Rueda, A., Méndez, F.J., Losada, I.J., 2016. An atmospheric-to-marine synoptic classification for statistical downscaling marine climate. Ocean Dynam. 66 https://doi.org/10.1007/s10236-016-1004-5.

Cannon, A.J., 2012. Regression-guided clustering: a semisupervised method for circulation-to-environment synoptic classification. J. Appl. Meteorol. Climatol. 51 https://doi.org/10.1175/JAMC-D-11-0155.1.

Chen, H.S., Houston, J.R., 1987. Calculation of water oscillation in an coastal harbors. HARBS and HARBD User's Manual. Rep. CERC-87-2, U.S. Army Eng. Waterw. Exp. Station. Vicksburg, MS.

Chen, H.S., Mei, C.C., 1974. Oscillations and wave forces in an offshore harbor - applications of hybrid finite element method to water-wave scattering. MIT Dep Civ Eng Ralph M, Parsons Lab Water Resour Hydrodyn Rep.

Cid, A., Castanedo, S., Abascal, A.J., Menéndez, M., Medina, R., 2014. A high resolution hindcast of the meteorological sea level component for Southern Europe: the GOS dataset. Clim. Dynam. 43, 2167–2184. https://doi.org/10.1007/s00382-013-2041-0.

Cornett, A., Wijdeven, B., Boeijinga, J., Ostrovsky, O., 2012. 3-D physical model studies of wave agitation and moored ship motions at ashdod port. In: 8th International Conference on Coastal and Port Engineering in Developing Countries. COPEDED, Chennai, India.

Danish Hydraulic Institute (DHI), 2017. MIKE 21 EMS. Elliptic Mild-Slope Wave Module. User Guide.

Danish Hydraulic Institute (DHI), 2022. MIKE 21 BW. Boussinesq Waves Module. User Guide.

Davidson, M.A., Huntley, D.A., Bird, P.A.d., 1998. A practical method for the estimation of directional wave spectra in reflective wave fields. Coast. Eng. 33 https://doi.org/10.1016/S0378-3839(98)00004-0.

De Girolamo, P., 1995. Computation of sea-wave direction of propagation of random waves. J. Waterw. Port, Coast. Ocean Eng. 121 https://doi.org/10.1061/(asce)0733-950x (1995)121:4(203).

de Jong, M.P.C., Borsboom, M.J.A., 2012. A practical post-processing method to obtain wave parameters from phase-resolving wave model results. Int. J. Ocean Clim. Syst. 3 https://doi.org/10.1260/1759-3131.3.4.203.

de Jong, M., Reijmerink, S., Capel, A., van der Hout, A., 2016. Combining Numerical Wave Models for Efficient Design of Port Layouts and Entrance Channels, vol. IX. PIANC-COPEDEC.

del Estado, Puertos, de Fomento, Ministerio, 1999. Recommendations for maritime works, Series 3, Planning, management and operation in port areas. ROM 3, 1–99 (-Design of the Maritime Configuration of Ports, Approach Channels and Harbour Basins).

Deltares, n.d. PHAROS.

Demenet, P.-F., Guisier, L., Marcol, C., 2018. Physical and numerical modelling of ships moored in ports. In: 34th PIANC World Congress.

Diaz-Hernandez, G., Mendez, F.J., Losada, I.J., Camus, P., Medina, R., 2015. A nearshore long-term infragravity wave analysis for open harbours. Coast. Eng. 97, 78–90. https://doi.org/10.1016/j.coastaleng.2014.12.009.

Diaz-Hernandez, G., Rodríguez Fernández, B., Romano-Moreno, E., L. Lara, J., 2021. An improved model for fast and reliable harbour wave agitation assessment. Coast. Eng. 170 https://doi.org/10.1016/j.coastaleng.2021.104011.

Donelan, M., Babanin, A., Sanina, E., Chalikov, D., 2015. A comparison of methods for estimating directional spectra of surface waves. J. Geophys. Res. C Oceans 120. https://doi.org/10.1002/2015JC010808.

Draycott, S., Davey, T., Ingram, D.M., Day, A., Johanning, L., 2016. The SPAIR method: isolating incident and reflected directional wave spectra in multidirectional wave basins. Coast. Eng. 114 https://doi.org/10.1016/j.coastaleng.2016.04.012.

Dusseljee, D., Klopman, G., Van Vledder, G., Riezebos, H.J., 2014. Impact of harbor navigation channels on waves: a numerical modelling guideline. Coast. Eng. Proc. 1 https://doi.org/10.9753/icce.v34.waves.58.

Egbert, G.D., Erofeeva, S.Y., 2002. Efficient inverse modeling of barotropic ocean tides. J. Atmos. Ocean. Technol. 19, 183–204. https://doi.org/10.1175/1520-0426(2002)019<0183:EIMOBO>2.0.CO;2.

Egbert, G.D., Bennett, A.F., Foreman, M.G.G., 1994. TOPEX/POSEIDON tides estimated using a global inverse model. J. Geophys. Res. 99 https://doi.org/10.1029/94jc01894.

Eikema, B.J.O., Attema, Y., Talstra, H., Bliek, A.J., De Wit, L., Dusseljee, D.W., 2018. Spectral modeling of wave propagation in coastal areas with a harbor navigation channel. PIANC-World Congr. Panama City 1–15.

Enet, F., Nahon, A., Vledder, G. Van, Hurdle, D., 2006. Evaluation of diffraction behind a semi-infinite breakwater in the SWAN Wave Model. Symp. Ocean Wave.

Espejo, A., Camus, P., Losada, I.J., Méndez, F.J., 2014. Spectral ocean wave climate variability based on atmospheric circulation patterns. J. Phys. Oceanogr. 44, 2139–2152. https://doi.org/10.1175/JPO-D-13-0276.1.

Frigaard, P., Andersen, T.L., 2014. Analysis of Waves: Technical Documentation for WaveLab 3.

GIOC, 2007. MSP Guide and Reference Manual. Ocean and Coastal Research Group. University of Cantabria, Spain, Version 1.0..

Gruwez, V., Bolle, a, Verwaest, T., Hassan, W., 2012. Numerical and physical modelling of wave penetration in Oostende harbour during severe storm conditions. In: 5th SCACR Int. Short Conf. Appl. Coast. Res. proceedings, 6th-9th June, 2011 - RWTH Aachen Univ. Ger. Mitteilungen des Lehrstuhls und Instituts für Wasserbau und Wasserwirtschaft der Rheinisch-Westfälischen Tech. H, vol. 165, pp. 198–205.

Guo, L., Ma, X., Dong, G., 2021. Performance accuracy of surfbeat in modeling infragravity waves near and inside a harbor. J. Mar. Sci. Eng. 9 https://doi.org/10.3390/jmse9090918.

Hanson, J.L., Tracy, B.A., Tolman, H.L., Scott, R.D., 2009. Pacific hindcast performance of three numerical wave models. J. Atmos. Ocean. Technol. 26, 1614–1633. https://doi.org/10.1175/2009JTECHO650.1.

Hashimoto, N., Kobune, K., 1987. Estimation of directional spectra from a Bayesian approach in incident and reflected wave field. Rep. PORT Harb. RES. INST. 26.

Holthuijsen, L.H., 2007. Waves in Oceanic and Coastal Waters, Waves in Oceanic and Coastal Waters. https://doi.org/10.1017/CBO9780511618536.

Holthuijsen, L.H., Herman, A., Booij, N., 2003. Phase-decoupled refraction-diffraction for spectral wave models. Coast. Eng. 49 https://doi.org/10.1016/S0378-3839(03)00065-6.

Huntley, D.A., Davidson, M.A., 1998. Estimating the directional spectrum of waves near a reflector. J. Waterw. Port, Coast. Ocean Eng. 124 https://doi.org/10.1061/(asce)0733-950x (1998)124:6(312).

Hurdle, D.P., Kostense, J.K., van den Bosch, P., 1989. Mild-slope Model for the Wave Behaviour in and Around Harbours and Coastal Structures in Areas of Variable Depth and Flow Conditions.

Svašek Hydraulics, 2019. Post-processing tool WAVEDIRECT [WWW Document]. URL. www.svasek.nl.

Iglesias, G., López, M., Carballo, R., Castro, A., Fraguela, J.A., Frigaard, P., 2009. Wave energy potential in Galicia (NW Spain). Renew. Energy 34. https://doi.org/10.1016/j.renene.2009.03.030.

Ilic, S., van der Westhuysen, A.J., Roelvink, J.A., Chadwick, A.J., 2007. Multidirectional wave transformation around detached breakwaters. Coast. Eng. 54 https://doi.org/10.1016/j.coastaleng.2007.05.002.

Isaacson, M., Qu, S., 1990. Waves in a harbour with partially reflecting boundaries. Coast. Eng. 14 https://doi.org/10.1016/0378-3839(90)90024-Q.

Isaacson, M., O'Sullivan, E., Baldwin, J., 1993. Reflection effects on wave field within a harbour. Can. J. Civ. Eng. 20 https://doi.org/10.1139/l93-054.

Isobe, M., Kondo, K., 1985. Method for estimating directional wave spectrum in incident and reflected wave field. In: Proceedings of the Coastal Engineering Conference. https://doi.org/10.1061/9780872624382.033.

Jammalamadaka, S. Rao, SenGupta, A., 2001. Topics in Circular Statistics. World Scientific.

Janssen, T.T., Van Dongeren, A.R., Kuiper, C., 2001. Phase resolving analysis of multidirectional wave trains. In: Proceedings of the International Symposium on Ocean Wave Measurement and Analysis. https://doi.org/10.1061/40604(273)39.

Kirby, J.T., Wei, G., Chen, Q., Kennedy, A., Dalrymple, R.A., 1998. FUNWAVE 1.0: Fully Nonlinear Boussinesq WaveModel Documentation and User's Manual. Res. CACR-98-06, Cent. Appl. CoastalResearch, Univ. Delaware.

Kostense, J.K., Meijer, K.L., Dingemans, M.W., Mynett, A.E., van den Bosch, P., 1986. Wave energy dissipation in arbitrarily shaped harbors of variable depth. Proc. 20 th. Int. Conf. Coast. Eng. 2002–2016.

Liu, P.L.F., Losada, I.J., 2002. Wave propagation modeling in coastal engineering. J. Hydraul. Res. 40 https://doi.org/10.1080/00221680209499939.

MarCom Working Group, 2012. Criteria for the (Un)loading of container vessels. PIANC Report 115.

MetOcean Solutions Ltd., 2018. Wavespectra. GitHub – Metocean/wavespectra.

Molina-Sanchez, R., Campos, Á., de Alfonso, M., de los Santos, F.J., Rodríguez-Rubio, P., Pérez-Rubio, S., Camarero-Orive, A., Álvarez-Fanjul, E., 2020. Assessing operability on berthed ships. common approaches, present and future lines. J. Mar. Sci. Eng. 8 https://doi.org/10.3390/JMSE8040255.

Mørk, G., Barstow, S., Kabuth, A., Pontes, M.T., 2010. Assessing the global wave energy potential. In: Proceedings of the International Conference on Offshore Mechanics and Arctic Engineering - OMAE. https://doi.org/10.1115/OMAE2010-20473.

NCSS, 2022. NCSS Statistical Software (Chapter 231). Circular Data Correlation.

Nortek, 2017. The Comprehensive Manual. Nortek Manuals.

Nwogu, O., Demirbilek, Z., 2001. BOUSS-2D: A Boussinesq Wave Model for Coastal Regions and Harbors.

Oude Vrielink, J., 2016. Bachelor Thesis: Improved Coupling Pharos-Diffrac. Including Spatial Variations in Wave Conditions along a Ship's Hull in Dynamic Mooring Analysis.

Panchang, V.G., Xu, B., 1995. CGWAVE: A Coastal Wave Transformation Model for Arbitrary Domains. Tech. Report, Dept. of Civil and Environmental Engineering, University of Maine.

Panicker, N.N., Borgman, L.E., 1970. Directional spectra from wave-gage arrays. Coast. Eng. Proc. 1 https://doi.org/10.9753/icce.v12.8.

Pascal, R., Bryden, I., 2011. Directional spectrum methods for deterministic waves. Ocean Eng. 38 https://doi.org/10.1016/j.oceaneng.2011.05.021.

Perez, J., Menendez, M., Losada, I.J., 2017. GOW2: a global wave hindcast for coastal applications. Coast. Eng. 124, 1–11. https://doi.org/10.1016/j.coastaleng.2017.03.005.

Pinheiro, L.V., Fortes, C.J.E.M., Santos, J.A., Fernandes, J.L.M., 2013. Numerical simulation of the behaviour of a moored ship inside an open coast harbour. In: Computational Methods in Marine Engineering V - Proceedings of the 5th International Conference on Computational Methods in Marine Engineering, MARINE 2013.

Portilla-Yandún, J., Cavaleri, L., Van Vledder, G.P., 2015. Wave spectra partitioning and long term statistical distribution. Ocean Model. 96 https://doi.org/10.1016/j.ocemod.2015.06.008.

Prislin, I., Zhang, J., 1996. Deterministic decomposition of irregular short-crested surface gravity waves. In: Proceedings of the International Offshore and Polar Engineering Conference.

Prislin, I., Zhang, J., Seymour, R.J., 1997. Deterministic decomposition of deep water short-crested irregular gravity waves. J. Geophys. Res. Ocean. 102 https://doi.org/10.1029/97JC00791.

Romano-Moreno, E., Diaz-Hernandez, G., Lara, J.L., Tomás, A., Jaime, F.F., 2022. Wave downscaling strategies for practical wave agitation studies in harbours. Coast. Eng. 175 https://doi.org/10.1016/j.coastaleng.2022.104140.

Rusu, E., Soares, C.G., 2013. Modeling waves in open coastal areas and harbors with phase-resolving and phase-averaged models. J. Coast Res. 29 https://doi.org/10.2112/JCOASTRES-D-11-00209.1.

Saha, S., Moorthi, S., Pan, H.L., Wu, X., Wang, Jiande, Nadiga, S., Tripp, P., Kistler, R., Woollen, J., Behringer, D., Liu, H., Stokes, D., Grumbine, R., Gayno, G., Wang, Jun, Hou, Y.T., Chuang, H.Y., Juang, H.M.H., Sela, J., Iredell, M., Treadon, R., Kleist, D., Van Delst, P., Keyser, D., Derber, J., Ek, M., Meng, J., Wei, H., Yang, R., Lord, S., Van Den Dool, H., Kumar, A., Wang, W., Long, C., Chelliah, M., Xue, Y., Huang, B., Schemm, J.K., Ebisuzaki, W., Lin, R., Xie, P., Chen, M., Zhou, S., Higgins, W., Zou, C. Z., Liu, Q., Chen, Y., Han, Y., Cucurull, L., Reynolds, R.W., Rutledge, G., Goldberg, M., 2010. The NCEP climate forecast system reanalysis. Bull. Am. Meteorol. Soc. 91, 1015–1057. https://doi.org/10.1175/2010BAMS3001.1.

Saha, S., Moorthi, S., Wu, X., Wang, J., Nadiga, S., Tripp, P., Behringer, D., Hou, Y.T., Chuang, H.Y., Iredell, M., Ek, M., Meng, J., Yang, R., Mendez, M.P., Van Den Dool, H., Zhang, Q., Wang, W., Chen, M., Becker, E., 2014. The NCEP climate forecast system version 2. J. Clim. 27, 2185–2208. https://doi.org/10.1175/JCLI-D-12-00823.1.

Sakakibara, S., Kubo, M., 2008. Effect of mooring system on moored ship motions and harbour tranquillity. Int. J. Ocean Syst. Manag. 1 https://doi.org/10.1504/IJOSM.2008.017783.

Sand, S.E., 1979. Three-dimensional Deterministic Structure of Ocean Waves.

Sand, S.E., 1984. Deterministic decomposition of pitch-and-roll buoy measurements. Coast. Eng. 8 https://doi.org/10.1016/0378-3839(84)90004-8.

Schäffer, H.A., Hyllested, P., 1994. Analysis of multidirectional waves using deterministic decomposition. In: Proc. Int. Symp. "Waves - Physical and Numerical Modelling", Vancouver. British Columbia, Canada, pp. 911–920.

Shi, F., Kirby, J., Tehranirad, B., Harris, J., Choi, Y.-K., Malej, M., 2016. FUNWAVE-TVD fully nonlinear Boussinesq wave model with TVD solver - documentation and user's manual (version 3.0). Cent. Appl. Coast. Res. Univ. Delaware.

Shih, H.H., 2012. Real-time current and wave measurements in ports and harbors using ADCP. In: Program Book - OCEANS 2012 MTS/IEEE Yeosu: the Living Ocean and Coast - Diversity of Resources and Sustainable Activities. https://doi.org/10.1109/OCEANS-Yeosu.2012.6263642.

Song, X., Ti, Z., Zhou, Y., 2022. Estimation of directional wave spectrum using measurement array pressure data on bottom-mounted offshore structure in incident and diffracted wave field. Shock Vib. 2022 https://doi.org/10.1155/2022/9764478.

Steward, D.R., Panchang, V.G., 2001. Improved coastal boundary condition for surface water waves. Ocean Eng. 28 https://doi.org/10.1016/S0029-8018(99)00054-2.

Svašek Hydraulics, n.d. HARES ("HArbour RESonance").

Teisson, C., Benoit, M., 1995. Laboratory measurement of oblique irregular wave reflection on rubble-mound breakwaters. In: Proceedings of the Coastal Engineering Conference. https://doi.org/10.1061/9780784400890.117.

Thoresen, C.A., 2003. Port Designer's Handbook: Recommendations and Guidelines. Thomas Telford Publishing. https://doi.org/10.1680/pdhrag.32286.

Tolman, H.L., 1991. A third-generation model for wind waves on slowly varying, unsteady, and inhomogeneous depths and currents. J. Phys. Oceanogr. 21 https://doi.org/10.1175/1520-0485(1991)021<0782:atgmfw>2.0.co;2.

Van der Ven, P.P.D., 2012. The Use of Numerical Models to Determine the Response of Moored Vessels to Waves in a Complex Harbour Geometry.

van der Ven, P., Reijmerink, B., van der Hout, A., de Jong, M., 2018. Comparison of validation studies of wave-penetration models using open benchmark datasets of Deltares. In: PIANC-world Congress Panama City.

van der Wiel, R.J., Kramer, J., van der Ven, P.P.D., Borsboom, M.J.A., de Jong, M.P.C., 2016. Influence of a parabolic reflector wall on the sea state in an array of point absorber wave energy converters. In: Progress in Renewable Energies Offshore - Proceedings of 2nd International Conference on Renewable Energies Offshore, RENEW 2016. https://doi.org/10.1201/9781315229256-48.

Van Essen, S., Van Der Hout, A., Huijsmans, R., Waals, O., 2013. Evaluation of directional analysis methods for low-frequency waves to predict LNGC motion response in nearshore areas. In: Proceedings of the International Conference on Offshore Mechanics and Arctic Engineering - OMAE. https://doi.org/10.1115/OMAE2013-10235.

Vicinanza, D., Contestabile, P., Ferrante, V., 2013. Wave energy potential in the north-west of Sardinia (Italy). Renew. Energy 50. https://doi.org/10.1016/j.renene.2012.07.015.

Vílchez, M., Clavero, M., Losada, M.A., 2016. Hydraulic performance of different non-overtopped breakwater types under 2D wave attack. Coast. Eng. 107, 34–52. https://doi.org/10.1016/j.coastaleng.2015.10.002.

Violante-Carvalho, N., Paes-Leme, R.B., Accetta, D.A., Ostritz, F., 2009. Diffraction and reflection of irregular waves in a harbor employing a spectral model. An. Acad. Bras. Cienc. 81 https://doi.org/10.1590/s0001-37652009000400019.

working group PTC II-24, 1995. Criteria for movements of moored ships in harbours: a practical guide (Supplement to bulletin No 88). In: PIANC - Permanent International Association of Navigation Congresses.

Yokoki, H., Isobe, M., Watanabe, A., 1995. On a method for estimating reflection coefficient in short-crested random seas. In: Proceedings of the Coastal Engineering Conference. https://doi.org/10.1061/9780784400890.054.

Zheng, Z., Ma, X., Ma, Y., Dong, G., 2020. Wave estimation within a port using a fully nonlinear Boussinesq wave model and artificial neural networks. Ocean Eng. 216 https://doi.org/10.1016/j.oceaneng.2020.108073.

Zheng, Z., Ma, X., Huang, X., Ma, Y., Dong, G., 2022. Wave forecasting within a port using WAVEWATCH III and artificial neural networks. Ocean Eng. 255 https://doi.org/10.1016/j.oceaneng.2022.111475.